



1 **Modelling bi-directional fluxes of methanol and**
2 **acetaldehyde with the FORCAsT canopy exchange model**

3

4 **Kirsti Ashworth¹, Serena H. Chung², Karena A. McKinney^{3*}, Ying Liu^{3**}, Bill J.**
5 **Munger^{3,4}, Scot T. Martin⁴ and Allison L. Steiner¹**

6 [1] Climate and Space Science and Engineering, University of Michigan, Ann Arbor, MI
7 48109, USA.

8 [2] Department of Civil and Environmental Engineering, Washington State University,
9 Pullman, WA 99164, USA.

10 [3] Department of Earth and Planetary Sciences, Harvard University, Cambridge, MA 02138,
11 USA.

12 [4] School of Engineering and Applied Sciences, Harvard University, Cambridge, MA 02138,
13 USA.

14 * Formerly of Department of Chemistry, Amherst College, Amherst, MA 01002

15 ^ Now at Peking University, China

16 Correspondence to: Kirsti Ashworth (ksashwor@umich.edu)

17 **Abstract**

18 The FORCAsT canopy exchange model was used to investigate the underlying mechanisms
19 governing foliage emissions of methanol and acetaldehyde, two short chain oxygenated
20 volatile organic compounds ubiquitous in the troposphere and known to have strong biogenic
21 sources, at a northern mid-latitude forest site. The explicit representation of the vegetation
22 canopy within the model allowed us to test the hypothesis that stomatal conductance regulates
23 emissions of these compounds to an extent that its influence is observable at the ecosystem-
24 scale, a process not currently considered in regional or global scale atmospheric chemistry
25 models.

26 We found that FORCAsT could only reproduce the magnitude and diurnal profiles of
27 methanol and acetaldehyde fluxes measured at the top of the forest canopy at Harvard Forest
28 if light-dependent emissions were introduced to the model. With the inclusion of such



1 emissions FORCAsT was able to successfully simulate the observed bi-directional exchange
2 of methanol and acetaldehyde. Although we found evidence that stomatal conductance
3 influences methanol fluxes and concentrations at scales beyond the leaf-level, particularly at
4 dawn and dusk, we were able to adequately capture ecosystem exchange without the addition
5 of stomatal control to the standard parameterisations of foliage emissions, suggesting that
6 ecosystem fluxes can be well enough represented by the emissions models currently used.

7 **Key points:** Canopy exchange model used to probe mechanisms controlling fluxes of
8 methanol and acetaldehyde; The effects of stomatal control of leaf-level emissions of
9 methanol and acetaldehyde emissions are not evident at the ecosystem scale; Bi-directional
10 exchange of oxygenated volatile organic compounds can be simulated by models that
11 explicitly and holistically consider canopy processes

12 **1 Introduction**

13 The exchange of many oxygenated volatile organic compounds (oVOCs) from forest canopies
14 has recently been observed to be bi-directional, with periods of strongly positive (i.e. up out
15 of the canopy to the atmosphere above) and negative (i.e. downward) fluxes (Park et al.,
16 2013; Karl et al., 2005; McKinney et al., 2011). Several of these compounds, e.g. acetone,
17 acetaldehyde, and methanol, are present in the atmosphere in large quantities (Singh et al.,
18 1995; Heikes et al., 2002; Millet et al., 2010; Jacob et al., 2002). They are also chemically
19 active, with acetone and acetaldehyde leading to the formation of PAN (peroxyacetyl nitrate)
20 and the transport of reactive nitrogen to remote regions (Fischer et al., 2014), and methanol
21 contributing significantly to the production of ground-level ozone (Tie et al., 2003). These
22 oVOCs have potentially important implications for regional air quality and climate modelling
23 and for estimating global atmospheric burdens of many trace gases (e.g. Folberth et al., 2006;
24 Fischer et al., 2014). However, many regional and global atmospheric chemistry and transport
25 models (CTMs) do not explicitly include dynamic biogenic sources and sinks of oVOCs.
26 While most now incorporate on-line calculations of biogenic emissions of isoprene and
27 monoterpenes, based on the light and temperature-dependence algorithms developed by
28 Guenther et al. (1995; 2006; 2012), methanol emissions have only been recently included in
29 some CTMs (e.g. GEOS-Chem; Millet et al., 2010; Laboratoire de Météorologie Dynamique
30 zoom (LMDz): Folberth et al., 2006) and most still rely on non-dynamic emissions
31 inventories for methanol and acetaldehyde if primary biogenic emissions of these species are
32 included (e.g. UKCA: O'Connor et al., 2014). Furthermore, Ganzeveld et al. (2008)



1 demonstrated the weaknesses of the algorithms currently used in 3-D chemistry transport
2 models to calculate primary emissions of methanol on-line. Similarly, dry deposition schemes
3 in CTMs are usually based on fixed deposition velocities (Wohlfahrt et al., 2015) or
4 calculated from roughness lengths and leaf area index values assigned to generic landcover
5 types (e.g. FRSGC-UCI: Wild et al., 2007; LMDz: Folberth et al., 2006). This simplistic
6 approach to biogenic sources and sinks may be a critical omission limiting their capability of
7 accurately simulating atmospheric composition in many world regions.

8 Here we focus on methanol and acetaldehyde, two oVOCs that are frequently observed in and
9 above forests but whose sources, sinks and net budgets are not known with any certainty
10 (Seco et al., 2007; Niinemets et al., 2004). While biogenic sources of both are strongly
11 seasonal, fluxes and concentrations can remain high throughout the growing season
12 (Stavrakou et al., 2011; Millet et al., 2011; Karl et al., 2003; Wohlfahrt et al., 2015).
13 Methanol fluxes are on the same order of magnitude as isoprene at many sites in the US (Fall
14 and Benson, 1996), suggesting their regional and global importance. The fundamental
15 mechanisms leading to the synthesis and/or subsequent release of methanol and acetaldehyde
16 are not currently fully understood (Karl et al., 2002; Seco et al., 2007).

17 Methanol is known to be produced from demethylation processes during cell wall expansion
18 and leaf growth with emissions peaking during springtime leaf growth and declining with leaf
19 age (Fall and Benson, 1996). The factors controlling its subsequent release to the atmosphere
20 are harder to decipher (Huve et al., 2007; Niinemets et al., 2004). Measurements at all scales
21 from leaf-level to branch enclosure and ground-based ecosystem-scale field measurements
22 (e.g. Kesselmeier et al., 2001; Karl et al., 2003; Seco et al., 2015; Wohlfahrt et al., 2015), as
23 well as satellite inversions (e.g. Stravakou et al., 2012) demonstrate a strong diurnal profile of
24 methanol fluxes similar to that of isoprene (e.g. Fall and Benson, 1996). Methanol synthesis,
25 unlike that of isoprene, is not specifically linked to photosynthesis and the light-dependence
26 observed in leaf-level emissions have been shown to result from regulation by the stomata due
27 to the high solubility of methanol in water (e.g. Nemecek-Marshall et al., 1995; Niinemets
28 and Reichstein, 2003a,b; Huve et al., 2007).

29 The pathways leading to both the synthesis and emission of acetaldehyde are not clear (Karl
30 et al., 2002; Jardine et al., 2008). Acetaldehyde has long been known to be an oxidation
31 product of ethanol produced in leaves under anoxic conditions (Kreuzwieser et al., 2000) but
32 this cannot explain the strong emissions observed under normal environmental conditions at



1 mid-latitude forests (e.g. Seco et al, 2007; Karl et al., 2003). Karl et al. (2003) observed that
2 bursts of acetaldehyde were emitted during light-dark transitions and postulated that such
3 emissions were associated with pyruvate decarboxylation. Leaf-level measurements of
4 acetaldehyde emissions have also been found to be tightly coupled to stomatal aperture (e.g.
5 Kreuzwieser et al., 2000; Karl et al., 2002; Niinemets et al., 2004) and it has been suggested
6 that this may account for observed light-dependent ecosystem-scale emissions of
7 acetaldehyde (Jardine et al., 2008).

8 Previous studies have suggested that the role of stomatal conductance in determining net flux
9 of oVOCs could be incorporated in large-scale models by adopting a compensation point
10 approach (see e.g. Harley et al., 2007; Ganzeveld et al., 2008; Jardine et al., 2008). The
11 compensation point for a given compound is the atmospheric concentration of that compound
12 at which the leaf, plant or canopy switches from acting as a net source to a net sink. While
13 firmly based in plant physiology and plant response to environmental conditions, this
14 approach would allow models lacking leaf-level processes to account for the changes in flux
15 direction (Harley et al., 2007; Ganzeveld et al., 2008). Observational (Jardine et al., 2008) and
16 modelling studies (Ganzeveld et al., 2008) have both shown the potential power of this
17 approach, although Jardine et al. (2008) found that the compensation point was heavily
18 dependent on light and temperature and may therefore not be straightforward to implement.

19 Here we use the FORCAsT (FORest Canopy-Atmosphere Transfer) canopy-atmosphere
20 exchange model (Ashworth et al., 2015) to investigate the key processes driving fluxes of
21 methanol and acetaldehyde, and explore possible underlying causes of their bi-directional
22 exchange. The model represents all within-canopy processes: primary emissions, chemical
23 and photolysis reactions, turbulent mixing and deposition. A particular strength of the
24 FORCAsT model is the inclusion of plant processes relevant to photosynthesis and
25 respiration; stomatal conductance is explicitly calculated by FORCAsT. We therefore focus
26 on exploring the role of primary biogenic emissions of methanol and acetaldehyde on canopy-
27 top fluxes. We assess the effectiveness of different representations of bVOC emissions
28 mechanisms in capturing ecosystem-scale fluxes. For the first time in a canopy exchange
29 model, we implement a mechanism by which stomatal conductance explicitly regulates
30 primary emissions in order to assess its role in governing primary emissions and influencing
31 ecosystem-scale bi-directional exchange of these key oVOCs. We compare modelled fluxes
32 using this mechanism with those from traditional empirical algorithms for direct and storage



1 emissions and with fluxes measured just above the top of the canopy at Harvard Forest in July
2 2012.

3 **2 Methods**

4 **2.1 Harvard Forest measurements**

5 Harvard Forest is situated in a rural area of Massachusetts, approximately 90 km from Boston
6 and 130 km from Albany. It is classified as a mixed deciduous broadleaved forest, with red
7 oak (36%) and red maple (22%) as the dominant species (McKinney et al., 2011). Continuous
8 measurements of micro-meteorological variables and air pollutants have been made from the
9 Environmental Monitoring Station (EMS) Tower, part of the AmeriFlux network, for 25 years
10 (Munger and Wofsy, 1999a,b). The tower, located at 42.5°N and 72.2°W and an elevation of
11 340 m, is 30 m high and is surrounded by primary forest with an average height of around 23
12 m. The long-term meteorological measurements include photosynthetically active radiation
13 (PAR), relative humidity (RH) and air temperature at multiple heights on the tower, together
14 with wind speed and direction recorded just below the top of the tower (at ~29 m) (Munger
15 and Wofsy, 1999a). In addition to exchanges of CO₂ collected to assess photosynthetic
16 activity and productivity, concentrations of CO at the top of the tower and fluxes of O₃ (at
17 multiple heights on the tower) are also routinely measured (Munger and Wofsy, 1999c). NO
18 and NO₂ concentrations and fluxes have been recorded in the past, with the most recent
19 measurements in 2002. In addition to these continuous atmospheric measurements, a suite of
20 other data is gathered periodically to determine ecosystem health and functioning. Such data
21 include leaf area index, tree girth, litter mass, leaf chemistry, and soil moisture and respiration
22 (Munger and Wofsy, 1999b).

23 Concentrations and fluxes of bVOCs and their oxidation products have also been measured at
24 the EMS Tower during several summer growing seasons (McKinney et al, 2011; Goldstein et
25 al., 1999; 1995), augmenting the Ameriflux suite of observations. Between 7th June and 24th
26 September 2012, a proton-transfer-reaction time-of-flight mass spectrometer (PTR-TOF-MS
27 8000, Ionicon Analytik GmbH, Austria) was used to measure the concentrations of volatile
28 organic compounds at the site. The PTR-TOF-MS is capable of the rapid detection of
29 hundreds of different VOCs at concentrations as low as a few pptv. PTR-TOF-MS has been
30 described previously by Jordan et al. (2009a, b) and Graus et al. (2010). The instrument
31 utilizes a high-resolution TOF detector (Tofwerk AG, Switzerland) to analyze the reagent and



1 product ions and allows for exact identification of the ion molecular formula (mass resolution
2 >4000).

3 Ambient air was sampled from an inlet mounted at the top of the 30-m EMS tower at a total
4 flow rate of 5 slpm using a configuration identical to that used by McKinney et al. (2011) in
5 2007. H_3O^+ reagent ions were used to selectively ionize organic molecules in the sample air.
6 The instrument was operated with a drift tube temperature of 60°C and a drift tube pressure of
7 2.20 mbar. The drift tube voltage was set to 550 V, resulting in an E/N of 126 Td (E, electric
8 field strength; N, number density of air in the drift tube; unit, Townsend, Td; 1 Td = 10^{-17} V
9 cm^2). PTR-TOF-MS spectra were collected at a time resolution of 5 Hz. Mass calibration was
10 performed every 2 min with data acquisition using the Tof-Daq v1.91 software (Tofwerk AG,
11 Switzerland). A calibration system in which gas standards (Scott Specialty Gases) were added
12 into a humidified zero air flow at controlled flow rates was used to establish the instrument
13 sensitivities to VOCs. Every 3 h the inlet flow was switched to pass through a catalytic
14 converter (platinum on glass wool heated to 350°C) to remove VOCs and establish
15 background intensities.

16 The PTR-TOF-MS captures the entire mass spectrum in each 5-Hz measurement, providing a
17 continuous mixing ratio time series at each mass-to-charge ratio rather than the disjunct time
18 series obtained in previous PTR-MS studies at this site (McKinney et al., 2011). As a result,
19 direct, rather than virtual disjunct, eddy covariances were determined and are reported herein
20 (Mueller et al., 2010). Wind speeds recorded at 8 Hz by a tri-dimensional sonic anemometer
21 located at the same height and less than 1 m away from the gas inlet were averaged to a 5-Hz
22 time base, synchronized with the mixing ratio data, and used in the eddy covariance
23 calculations. Eddy covariance fluxes were calculated from the data for 30-minute intervals
24 using methods described in McKinney et al. (2011). Ambient mixing ratios were averaged
25 over the same 30-minute intervals for which fluxes were calculated. The 30-minute average
26 mixing ratios and fluxes were then binned by time of day to calculate diurnal averages.

27 Eddy covariance is a powerful technique for the direct detection and estimation of ecosystem-
28 scale fluxes of trace gases within and above vegetation canopies (see reviews by Baldocchi,
29 2003; 2014). However, its reliability for measuring night-time fluxes can be low (Gu et al.,
30 2005; Baldocchi, 2014; Goulden et al., 1996; Jarvis et al., 1997). Its successful application
31 relies on assumptions of steady-state conditions, conditions that do not always exist at night
32 (see e.g. Baldocchi, 2003). The night-time formation of a stable atmospheric layer near the



1 surface can result in stratification, trapping trace gases below the instrument detection height
2 and altering the footprint of the flux measurement (Gu et al. 2005; Baldocchi, 2003) leading
3 to high associated errors in flux estimation (Goulden et al., 1996). While we acknowledge that
4 the magnitudes of the recorded night-time fluxes during summer 2012 may have large
5 associated errors, we are confident in the direction of the exchange as we see variation
6 between different species suggesting no systematic bias.

7 Isoprene, total combined monoterpenes, MVK and MACR (detected as a single combined
8 species), methanol, acetaldehyde and acetone were all detected at concentrations well above
9 the PTR-MS detection limit and determined to be free from interference from other
10 compounds (McKinney et al., 2011). Here we confine our analysis to concentrations and
11 fluxes of methanol and acetaldehyde. Table 1 summarises the relevant flux, concentration and
12 meteorological measurements made at the EMS tower during the summer of 2012.

13 **2.2 FORCAsT1.0 canopy exchange model**

14 FORCAsT (version 1.0) is a single column (1-D) model that simulates the exchange of trace
15 gases and aerosols between the forest canopy and atmosphere. A full description of
16 FORCAsT is given in Ashworth et al. (2015). Here we provide a brief overview, summarise
17 biogenic emissions and flux calculations in the model and describe the simulations performed.

18 FORCAsT1.0 has 40 vertical levels of varying thickness extending to a height of ~4 km, with
19 the highest resolution nearest the ground where the complexity is greatest, i.e. within the
20 canopy space. Micro-meteorological conditions (temperature, PAR, RH) within the canopy
21 are determined prognostically by energy balance, accounting for the physical structure of the
22 canopy. The gas-phase chemistry scheme incorporated in FORCAsT1.0 is a modified version
23 of the CalTech Chemical Mechanism (CACM; Griffin et al., 2002; 2005; Chen and Griffin,
24 2005), which includes 300 species whose concentrations are solved at every chemistry
25 timestep (currently 1 minute), plus O₂ and water vapour (Ashworth et al., 2015). Ninety-nine
26 of the species are assumed to be condensable, and are lumped into 11 surrogate groups based
27 on similar volatility and structure. Aerosol-phase concentrations of these surrogate groups are
28 also calculated at every timestep based on equilibrium partitioning (Ashworth et al., 2015;
29 Chen and Griffin, 2005).

30 The CACM chemistry mechanism in FORCAsT treats methanol as an individual species,
31 although its reactions are limited to oxidation by OH to produce formaldehyde. Acetaldehyde



1 is not treated individually but is instead mapped to a lumped group of aldehydes (ALD1, with
2 $<C_5$). The oxidation reactions for this group are based on acetaldehyde and no other species is
3 currently emitted into the ALD1 group. Acetaldehyde has a far greater number of chemical
4 sources and sinks in the FORCAsT simulations of a forest environment than methanol. See
5 Ashworth et al. (2015) for details of the reactions and reaction rates included in FORCAsT.

6 FORCAsT incorporates dry deposition of all species based on the resistance scheme of
7 Wesely (1989) and modified by Gao et al. (1993). The scheme assumes that the rate of
8 deposition of a compound to canopy surfaces is determined by atmospheric, boundary and
9 surface resistances operating in series or parallel analogous to electrical resistances.
10 Atmospheric and surface boundary layer resistances are common to all chemical species and
11 are dependent on turbulence. As FORCAsT includes an explicit representation of the canopy,
12 the surface resistance term includes cuticular, mesophylllic and stomatal resistances which are
13 dependent on the physic-chemical properties of the depositing species as well as the light,
14 temperature and water potential of the leaf. The deposition scheme described in Ashworth et
15 al. (2015) and Bryan et al. (2012) has been updated to include methanol. The deposition
16 velocity of acetaldehyde is calculated using parameters for the lumped ALD1 group, and the
17 parameters for ALD1 and methanol deposition are shown in Table 3.

18 While a 1-D model cannot capture horizontal transport, FORCAsT does include a simple
19 parameterisation to account for advection (Bryan et al., 2012; Ashworth et al., 2015). For the
20 simulations here, only advection of NO_2 is considered such that a NO_2 mixing ratio of 1 ppbv
21 is set just above the canopy based on average midday (defined as 10:00-17:00 EST) NO_x and
22 NO_y (total reactive nitrogen species) concentrations. While nitrogen species were not
23 measured at Harvard Forest in 2012, concentrations reported from the site by Moody et al.
24 (1998) are extrapolated to 2012 using July monthly average NO_x levels measured at the
25 nearby US EPA monitoring station at Ware 42.3°N, 72.3°W, elevation 312 m (roughly 30 km
26 southwest of the EMS Tower). This scaling accounts for the observed decrease in NO_x levels
27 across the region as a result of emission reduction strategies (see e.g. EPA, 2015). All NO_x is
28 assumed to be advected as NO_2 . The initial concentration of N_2O_5 at 29 m was set to give an
29 average $NO_x:NO_y$ ratio of 0.4 (Moody et al., 1998), assuming all residual NO_y to be N_2O_5
30 initially.



1 **2.2.1 Flux calculations**

2 Fluxes of gases and particles are calculated to be proportional to both the concentration
3 gradient and the efficiency of vertical mixing between adjacent model layers (Eq. 1). Upward
4 fluxes are modelled as positive and occur when the concentration of a particular species is
5 higher at a lower height. The flux, F_i ($\text{kg m}^{-2} \text{s}^{-1}$) of an individual species, i , between two
6 model levels is given by:

$$7 \quad F_i = -K_H \frac{\Delta C_i}{\Delta z}, \quad (1)$$

8 where K_H is the eddy diffusivity ($\text{m}^2 \text{s}^{-1}$), ΔC_i the difference in mass concentrations (kg kg^{-1})
9 at the mid-height of the levels, and Δz the difference in height (m) between the levels. Eddy
10 diffusivity, concentrations of all gas-phase and aerosol species, and fluxes are calculated at 1-
11 minute timesteps. The eddy diffusivity at the instrument height of 29 m is constrained by
12 observed windspeeds (Bryan et al., 2012).

13 Modelled fluxes should be viewed as an instantaneous snapshot, both temporally and
14 spatially, as the calculation relies heavily on the concentration gradient across an arbitrary
15 boundary level, in this case the instrument height of 29 m. Actual concentration gradients
16 display rapid fluctuations (see e.g. Steiner et al., 2011) due to heterogeneity in emissions (see
17 e.g. Bryan et al., 2015) and chemistry (see e.g. Butler et al., 2008), as well as the occurrence
18 of coherent structures which can result in counter-gradient flow of matter (Steiner et al., 2011
19 and references therein).

20 **2.2.2 Biogenic emissions**

21 Emissions of VOCs from vegetation can be described as following one of two possible routes
22 (Grote and Niinemets, 2008). In the first, the compound is released to the atmosphere
23 immediately on production (e.g. isoprene). Such emissions are tightly coupled to
24 photosynthesis and are therefore dependent on both temperature and light, falling to zero at
25 night. We refer to such emissions as “direct”. In the second pathway, VOCs are stored in
26 specialist structures within the plant after their production (e.g. monoterpenes). Emissions
27 from these storage pools occur by diffusion and are controlled by temperature alone. We term
28 these “storage” emissions. It is thought that emissions of oVOCs are a combination of these
29 (“combo”), with a proportion released directly on synthesis and the remaining fraction
30 emitted from storage pools.



1 Emission rates are calculated in FORCAsT by modifying basal emission factors (rates at
2 standard conditions, usually 30°C and 1000 $\mu\text{mol m}^{-2} \text{s}^{-1}$ of PAR) according to empirical
3 relationships describing their dependence on light and temperature. These modifications
4 (referred to as activity factors) follow the standard parameterisations of Guenther et al. (1995;
5 2012). For storage emissions, which are modelled as dependent on temperature only, the
6 activity factor is a simple exponential relationship:

$$7 \quad \gamma_T = e^{-\beta(T_L - T_S)}, \quad (2)$$

8 where γ_T is the temperature-dependent activity factor for storage emissions, β the temperature
9 response factor (K^{-1}), T_S is 293K, T_L (K) the leaf temperature (see Guenther et al., 2012). For
10 further details of the activity factors for direct emissions included in FORCAsT the reader is
11 referred to Ashworth et al. (2015) and references therein.

12 **2.2.3 Stomatal resistance**

13 FORCAsT includes a physical representation of a forest canopy, with the lowest eight model
14 levels set as trunk space and the next ten as crown space. The ten crown space levels contain
15 the foliage; the total leaf area estimated for 2012 based on litter fall is distributed among the
16 levels according to balloon measurements made at the site by Parker (1999). Within each
17 crown space level, the leaves are assigned to one of nine equally-spaced angle classes
18 assuming a spherical canopy based on leaf normal angle (Goel et al., 1989) and the fraction of
19 shaded leaf area calculated. Photosynthetic parameters, including stomatal resistance, are then
20 calculated for each leaf angle class at each level within the crown space. The stomatal
21 conductance (inverse of stomatal resistance) describes the aperture of the stomata and
22 determines evapo-transpiration (hence heat flux and energy balance) and deposition rates
23 within FORCAsT. It is not currently used to control the rate of biogenic emissions.

24 Stomatal resistance is modelled according to leaf temperature, PAR, water potential and
25 vapour pressure deficit using the relationships developed by Jarvis (1976) as described by
26 Baldocchi et al. (1987). The overall stomatal resistance (r_s) is the product of these individual
27 factors (Eq. 3) which are summarised below in Eqs. 4-8

$$28 \quad R_s = r_{s\text{min}} \cdot r_s(\text{PAR}) \cdot r_s(T) \cdot r_s(D) \cdot r_s(p), \quad (3)$$

29 where $r_s(\text{PAR})$ is the response of stomatal resistance to changes in PAR, $r_{s\text{min}}$ (s m^{-1}) is the
30 minimum stomatal resistance and b_{rs} is an empirical coefficient:



$$1 \quad r_s(\text{PAR}) = r_{s\text{min}} \left(1 + \frac{b_{rs}}{\text{PAR}} \right), \quad (4)$$

2 and $r_s(T)$ is the response of stomatal resistance to changes in leaf temperature (T_{lf} , °C), T_{min} ,
 3 T_{max} , and T_0 are the minimum and maximum temperatures for stomatal opening and optimum
 4 temperature respectively:

$$5 \quad r_s(T) = \left\{ \left(\frac{T_{\text{lf}} - T_{\text{min}}}{T_0 - T_{\text{min}}} \right) \left(\frac{T_{\text{max}} - T_{\text{lf}}}{T_{\text{max}} - T_0} \right)^{b_T} \right\}^{-1}, \quad (5)$$

$$6 \quad b_T = \left(\frac{T_{\text{max}} - T_0}{T_{\text{max}} - T_{\text{min}}} \right), \quad (6)$$

7 and $r_s(D)$ is the relationship between stomatal resistance and vapour pressure deficit (D ;
 8 mbar), and b_v is an empirical coefficient:

$$9 \quad r_s(D) = \left(1 + \frac{b_v}{D} \right)^{-1}, \quad (7)$$

10 Water potential is assumed to act only once a threshold value is reached. Above this value it is
 11 modelled as:

$$12 \quad r_s(\varphi) = \left(\frac{1}{a \cdot \varphi + b_w} \right), \quad (8)$$

13 where φ is the water potential (bar), and a and b_w are constants. Below the water potential
 14 threshold $r_s(\varphi)$ is taken as unity. The values of the constants used in these calculations are
 15 shown in Table 4.

16 Stomatal resistance is only calculated in FORCAst during the day (defined within FORCAst
 17 as $\text{PAR} \geq 0.01 \text{ W m}^{-2}$); at night stomatal resistance is assumed equal to the minimum cuticular
 18 resistance (3000 s m^{-1}).

19 **2.3 FORCAst simulations**

20 All model simulations were performed for an average day in July 2012, the middle of the
 21 growing season, to ensure measurement data did not include either the spring burst of
 22 methanol nor elevated acetaldehyde emissions during senescence. FORCAst was initiated
 23 with site-specific parameters and measurements of the physical structure of the canopy and
 24 environmental conditions (Table 2). Initial meteorological conditions and atmospheric
 25 concentrations of chemical species were taken from the 2012 EMS tower data (see Table 2).
 26 Initial air temperature above the canopy is calculated on-line using the average lapse rate
 27 observed by the radiosonde at Albany (the nearest sounding station, ~90 km from Harvard



1 Forest), and within the canopy by interpolation with the 2-m temperature reading.
2 Concentrations of O₃ within the canopy are based on observations from the EMS tower, and
3 above the canopy follow a typical night-time profile as described in Forkel et al. (2006).
4 Concentrations of other species are assumed to decay exponentially with height such that the
5 e-folding height is 100 m for short-lived species and 1000 m for longer-lived compounds. All
6 model simulations started at 00:00 EST and continued for 48 hours, with the same driving
7 data used for each 24 hour period and analysis confined to the second day to account for
8 model spinup.

9 In addition to a baseline simulation, we perform a series of simulations that represent the
10 potential bVOC emissions routes using the “traditional” algorithms based on the observed
11 light and/or temperature dependence encapsulated in the MEGANv2.1 model of Guenther et
12 al. (2012); see Section 2.2.2. We then introduce stomatal control to the temperature-only
13 dependent emissions (i.e. those from storage pools) to determine whether the observed leaf-
14 level regulation of the emissions of oVOCs by stomatal aperture affects ecosystem-scale
15 fluxes (Section 2.3.3). A final series of sensitivity tests explores the extent to which stomatal
16 control governs canopy-top fluxes (Section 2.3.3). Table 5 summarises the simulations and
17 sensitivity tests.

18 Model performance was evaluated against average fluxes and concentrations measured at 29
19 m throughout July 2012 at Harvard Forest. The raw measurement data were grouped and
20 averaged for each model output time for the duration of the campaign period to create
21 “typical” diurnal profiles of methanol and acetaldehyde fluxes and concentrations. The flux
22 data in particular exhibited large variability introducing high uncertainty to the assessment.
23 Observations of both fluxes and concentrations of acetaldehyde were more variable than those
24 of methanol, reflecting the greater number of chemical sources and sinks of acetaldehyde in
25 conjunction with lower emission rates. The observations referred to throughout the main text
26 and shown in Fig. 4, 6 and 7 are these averages of the campaign data.

27 **2.3.1 Baseline**

28 All simulations were driven using meteorology for an average July day with initial conditions
29 set to July average values for all variables at 00:00 EST (shown in Table 2). For the baseline
30 simulation, default FORCAsT settings for emissions, dry deposition and chemical production
31 and loss (Ashworth et al., 2015) were used; the default FORCAsT settings do not consider



1 primary emissions of methanol and acetaldehyde. Only primary emissions of isoprene and the
2 monoterpenes α -pinene, β -pinene and *d*-limonene are included in the base case, with emission
3 factors (Table 6a) based on average rates for mixed deciduous woodland in N America
4 (Geron et al., 2000; Helmig et al., 1999).

5 **2.3.2 Primary emissions sensitivity tests**

6 Simulations including primary emissions of methanol and acetaldehyde were conducted to
7 understand the effect of adding primary emissions of oVOC. The specific changes from the
8 baseline are described below and summarised in Table 5.

9 In the first three “emissions” (E-) simulations, primary emissions of methanol and
10 acetaldehyde are included: firstly with all emissions assumed to be direct (E-direct), then all
11 from storage pools (E-storage), and finally as a combination of the two with 80% taken to be
12 direct and the remainder storage (E-combo). Emission rates for methanol and acetaldehyde
13 (Table 5) were initially based on standard emission factors for methanol and bidirectional
14 VOCs, respectively, for temperate deciduous broad-leaved trees given by Guenther et al.
15 (2012) and scaled for this site by isoprene emission factor. The emission factors were then
16 modified to best reconcile modelled and observed concentrations and fluxes at 29 m whilst
17 ensuring that total canopy emissions for all simulations were within $\pm 10\%$. The proportion of
18 80% direct and 20% storage emissions included in E-combo was also based on the “light-
19 dependent fractions” assigned to methanol and bidirectional VOCs by Guenther et al. (2012).
20 A sensitivity test with the combination of 90% direct and 10% storage (E-combo90) was also
21 performed. For each simulation, emission factors and total emissions are listed in Table 6b,
22 and diel profiles of total emissions, deposition and canopy chemical production and loss are
23 shown in Fig. 1. While the general pattern of emissions is the same in all simulations (Figs.
24 1a,b), the magnitude of the midday peak and overnight emission rate vary between the
25 different emission pathways introduced. The greater the contribution from storage the higher
26 the overnight and the lower the daytime peak with E-direct (green line; 0% storage emissions)
27 and E-storage (blue line; 100% storage) representing the extreme cases. Changes in emission
28 rates alter the concentrations of methanol or acetaldehyde within the crown space driving
29 differences in both dry deposition (Figs. 1c,d) and chemical production and loss (Figs. 1e,f)
30 rates. Fig. 1 further demonstrates the relatively small contribution of chemical production and
31 loss to the canopy space budgets of methanol and acetaldehyde.



1 2.3.3 Stomatal control sensitivity tests

2 Previous theoretical and laboratory-based studies have demonstrated the importance of
 3 stomatal aperture in the regulation of emissions of oVOCs from storage structures (e.g.
 4 Niinemets and Reichstein, 2003a,b; Nemecek-Marshall et al., 1995; Huve et al., 2007; Karl et
 5 al., 2002). Controlled experiments and leaf-level measurements suggest that emissions of
 6 many VOCs are dependent on stomatal conductance, although the extent to which the stomata
 7 regulate emission rates is highly dependent on both the compound and the leaf structure
 8 (Niinemets and Reichstein, 2003a).

9 Further sensitivity tests were performed specifically to test the dependence of the emissions of
 10 methanol and acetaldehyde on stomatal conductance. Stomatal resistance (the reciprocal of
 11 conductance) is explicitly calculated for every canopy level at every model timestep based on
 12 incident PAR, leaf temperature and water potential (Eq. 3). In this series of tests, the
 13 calculated resistances were used to scale the temperature-dependence of storage emissions of
 14 methanol and acetaldehyde (given in Eq. 2) for both the storage and combo emission
 15 pathways as shown in Eq. 9.

$$16 \quad \gamma_{TR} = \gamma_T \cdot R_{fct} = e^{-\beta(T_L - T_S)} \cdot R_{fct}, \quad (9)$$

17 where R_{fct} is a stomatal control factor.

18 In the first of the “stomatal control” (S-) sensitivity tests, R_{fct} increased proportionally with
 19 stomatal conductance (i.e. inversely with stomatal resistance) as shown in Eq. 10:

$$20 \quad R_{fct} = \frac{3000}{n \cdot R_{stom}}, \quad (10)$$

21 where R_{stom} ($(\mu\text{mol m}^{-2} \text{s}^{-1})^{-1}$) is the stomatal resistance, 3000 is the limiting night-time value
 22 of R_{stom} and n is a scaling factor, which was initially set to 3 for the S-storage and S-combo
 23 simulations. The effect of the choice of value of n is explored in Section 3.5.

24 Fig. 2 shows the diel cycle of stomatal resistances calculated in FORCAST for each model
 25 level within the crown space; an average canopy resistance is also indicated. R_{stom} is set to
 26 3000 overnight and falls to a minimum during the middle of the day when light levels are
 27 highest in the canopy. R_{stom} is lower at the top of the canopy and increases with increasing
 28 depth into the foliage layers. The profile of R_{fct} (Eq. 10) describes the inverse of R_{stom} ,
 29 reaching a peak at midday and having a greater value higher in the canopy. As shown in the
 30 middle panels R_{fct} reaches >1.0 during the middle of the day for all but the very lowest canopy



1 layers. Modelled stomatal control (S- simulations) therefore enhances emissions of methanol
2 and acetaldehyde above those simulated by traditional emissions algorithms during this time.
3 There is evidence that this may be biologically realistic with stomatal aperture limiting
4 emissions from storage pools and leading to increased pool size and hence greater
5 concentration gradients between plant tissue and the surrounding atmosphere (see e.g. Jardine
6 et al., 2008). This in turn drives an increase in emissions above those predicted based on
7 synthesis rates of oVOC. However, traditional emissions models were derived to fit observed
8 emission rates (see e.g. Guenther et al., 1993) and could be assumed to account for this effect.
9 Hence, a second set of “modified” stomatal control (R-) experiments was performed in which
10 it was assumed that beyond a threshold stomatal aperture, stomatal conductance no longer
11 controls emissions, which continue unhindered once the stomates are considered to be fully
12 open. Beyond this threshold emissions from storage pools are regulated by temperature alone
13 according to the relationship in Eq. 2, i.e. R_{fct} in Eq. 9 takes a value of unity, thus assuming
14 that “traditional” emissions algorithms correctly capture emission rates during the middle of
15 the day. Within FORCAsT this was modelled using a threshold function:

$$16 \quad R_{fct} = \frac{3000}{n \cdot R_{stom}}, R_{fct} < 1.0 \quad (11a)$$

$$17 \quad R_{fct} = 1.0, \quad \text{at all other times} \quad (11b)$$

18 The use of the function shown in Eqs. 11a and 11b limits the temporal extent of stomatal
19 control on methanol and acetaldehyde emissions for most canopy layers to the transition times
20 of day (dawn and dusk) when the stomata are either opening or closing as light levels increase
21 or decrease. This is consistent with results from controlled experiments and observations by
22 Niinemets and Reichstein (2003a) that indicate that stomatal aperture has only a transient
23 effect on the emissions of oVOC and is negligible under steady-state light conditions. It
24 should be noted however that under the average July radiation conditions the lower canopy
25 levels do not receive sufficient PAR to reach this threshold value within FORCAsT.

26 **3 Results**

27 **3.1 Summary of observations**

28 July was roughly the middle of the growing season in 2012 with emissions unaffected by
29 springtime leaf flush or autumn senescence. As observed previously at many sites, fluxes of
30 both methanol and acetaldehyde are highly variable with periods of net positive and net



1 negative exchange (e.g. McKinney et al., 2011; Wohlfahrt et al., 2015; Karl et al., 2005). In
2 prior years, concentrations of methanol at Harvard Forest remained high even outside of the
3 spring emissions peak (McKinney et al., 2011).

4 Fig. 3 shows correlations of the observed daytime (05:00-19:00 EST) fluxes of methanol and
5 acetaldehyde during July 2012 with air temperature, PAR, canopy stomatal conductance, and
6 concentrations of methanol and acetaldehyde respectively. Canopy stomatal conductance for
7 the tower footprint was estimated from energy fluxes measured at Harvard Forest following
8 the methodology of Shuttleworth et al. (1984) to calculate surface resistances. The raw data
9 were highly scattered, and were therefore binned by the independent variable in each case
10 with Fig. 3 showing only the mean values (with bars showing ± 1 standard deviation to give an
11 indication of the variability of the data) for each of these bins for clarity. The weak
12 relationships with each of the environmental variables evident in Fig. 3 illustrate the difficulty
13 in identifying the key processes driving canopy-scale exchanges of oVOC under varying
14 environmental conditions from observations alone.

15 Canopy-top fluxes of methanol appear to be positively correlated with temperature (Fig. 3a)
16 and to a lesser extent with PAR (Fig. 3c). The correlation with temperature seems to be
17 exponential as might be expected. The contribution of stomatal conductance to observed
18 methanol fluxes is more difficult to interpret although the data appear to show a strong linear
19 correlation at low conductance, suggesting that at small stomatal aperture the stomata exert
20 control over fluxes of methanol to the extent that it is observable at the canopy scale. A
21 similar relationship between canopy-top methanol fluxes and concentrations is likely due to
22 the influence of atmospheric concentrations on dry deposition to surfaces within the canopy.

23 Fluxes of acetaldehyde are lower and more variable than those of methanol, and averages are
24 clustered near zero. However, they do appear to be positively correlated with temperature
25 (Fig. 3b) although the relationship is weaker and does not appear to be exponential. There is
26 no discernible correlation between acetaldehyde fluxes and either PAR (Fig. 3d) or stomatal
27 conductance (Fig. 3f). This might suggest that acetaldehyde emissions are not controlled by
28 stomatal aperture but may rather indicate the influence of the greater number of sources and
29 sinks for acetaldehyde at the spatial and temporal scale of the canopy. Jardine et al. (2008)
30 describe a clear negative correlation between acetaldehyde fluxes and concentrations
31 measured in the laboratory and Fig. 3h could be interpreted in a similar way although the
32 correlation here (at the canopy scale) is far weaker.



1 The weakness of the observed correlations and variability of the observed fluxes are a
2 reflection of the complexity of in-canopy processes and interactions, all of which (emissions,
3 photo-chemical production and loss, and turbulent exchange) are strongly influenced by
4 temperature while only photolysis and direct foliage emissions are directly dependent on light
5 levels (although the penetration of radiation into the canopy drives both leaf temperature and
6 turbulence).

7 **3.2 Baseline**

8 When FORCAsT is driven in default mode with average meteorology and initial conditions
9 for July 2012 and only primary emissions of isoprene and monoterpenes, the model fails to
10 capture either the magnitude or diurnal profile of the observed concentrations and fluxes of
11 methanol and acetaldehyde at 29 m (Fig. 4(a)-(d); black lines). For both methanol and
12 acetaldehyde FORCAsT simulates negative fluxes at all times, with a pronounced decrease
13 during daylight hours (Fig. 4(a) and (c)). Fluxes measured by eddy covariance by contrast
14 show strongly positive (upward) exchange occurring during the day and fluxes near zero at
15 night. Observed concentrations increase to 12.8 ppbv (methanol) and 0.72 ppbv
16 (acetaldehyde) during daylight hours, dipping sharply after dusk and decreasing steadily to a
17 minimum around dawn (Fig. 4(b) and (d)). The baseline modelled concentrations of both
18 compounds decrease throughout the 24-hour period, with a dip soon after dawn, and a slight
19 increase during the early afternoon (Fig. 4(b) and (d)), the latter most likely a result of an
20 increase in net chemical production. The measurements indicate strong daytime sources of
21 both methanol and acetaldehyde within the canopy, which FORCAsT does not simulate with
22 the default model settings.

23 **3.3 Biogenic emissions of methanol and acetaldehyde ('E-' simulations)**

24 The pronounced diurnal profile of the observed methanol fluxes with a midday peak is
25 strongly reminiscent of light and temperature dependent biogenic emissions similar to
26 isoprene. Leaf-level measurements of methanol emissions have demonstrated that all C₃
27 vegetation types emit methanol at rates on a par with the major terpenoids (Fall and Benson,
28 1997). Given the lack of other in-situ sources of methanol, the diel cycle of fluxes and
29 concentrations which is generally absent from anthropogenic and transported sources, and the
30 magnitude of the underestimation of canopy-top fluxes (ranging from ~0.01 overnight to 0.7



1 mg m⁻² h⁻¹ in the early afternoon), it seems likely that there are substantial foliage emissions
2 of methanol at Harvard Forest (see also McKinney et al., 2011).

3 While the magnitude of the missing acetaldehyde fluxes is lower (between ~0.01 and 0.05 mg
4 m⁻² h⁻¹), the diel cycles of both fluxes and concentrations is similar to those of methanol. This
5 again suggests relatively strong leaf-level emissions of acetaldehyde at this site. It is likely
6 that the absolute concentrations and fluxes are lower as primary emissions of acetaldehyde
7 have generally been found to be a factor of 2-10 lower than those of methanol (Seco et al.,
8 2007; Karl et al., 2003; Guenther et al., 2012) and acetaldehyde has chemical sources and
9 sinks that are relevant at the timescale of canopy exchange.

10 Fig. 5 shows the relative contributions of the competing processes driving the evolution of
11 methanol and acetaldehyde within and just above the canopy over the course of the day for
12 the E-combo90 and E-combo simulations respectively. Concentrations of both oVOC (Fig. 5a
13 and 3g) increase strongly at all levels from a minimum around dawn. In the case of methanol
14 (Fig. 5a) there is a clear maximum just below the top of the canopy corresponding to the most
15 densely foliated level where emissions also peak. This feature is less evident in the case of
16 acetaldehyde (Fig. 5g) demonstrating its greater number of sources and sinks. Chemical
17 production and loss is highest at the top of the canopy and the boundary layer just above due
18 to the higher levels of radiation and temperature driving OH radical formation and reaction
19 rates. For both oVOC it is emissions and deposition, both leaf-level processes governed by the
20 stomata, that dominate production and loss; chemistry contributions are at least an order of
21 magnitude lower. However, both chemistry and turbulent transport contribute to the
22 complexity evident in the evolution of concentrations and fluxes and the high degree of
23 variability seen in the observations (see e.g. Figs. 3 and 5).

24 Difficulties in simultaneously reconciling both fluxes and concentrations of methanol and
25 acetaldehyde are also likely a result of the complexity of in-canopy processes. Fig. 5 shows
26 that the top of the canopy is a region of abrupt transition for the sources and sinks of oVOC
27 with emissions and deposition limited to the canopy and a sudden change in turbulent mixing
28 above the foliage. The instantaneous nature of concentrations, concentration gradients and
29 fluxes of methanol and acetaldehyde in time and space are evident from Fig. 5 which
30 demonstrates that the level at which model and measurements are compared can also affect
31 the measured-modeled bias, an effect compounded by the instantaneous nature of the model
32 output fluxes (Eq. 1).



1 3.3.1 Methanol

2 The effect of introducing the different mechanisms of methanol emissions (simulations E-
3 direct, E-storage, E-combo; Table 5) on fluxes and concentrations of methanol are shown in
4 Fig. 4(a) and (b). Storage emissions are dependent only on temperature and therefore remain
5 relatively high overnight. While modelled fluxes of methanol are positive when storage
6 emissions are included and peak during the middle of the day, modelled midday fluxes are
7 only around a third of measured fluxes (Fig. 6(a); E-storage) and modelled night-time fluxes
8 are well above ($\sim 0.15\text{--}0.20\text{ mg m}^{-2}\text{ h}^{-1}$) those observed which are close to but slightly below
9 zero. The diurnal profile of E-storage modelled concentrations is the inverse of measured
10 methanol mixing ratios: elevated at night and decreasing toward the middle of the day (Fig.
11 6(b); E-storage). This gives further credence to the light-dependent nature of methanol
12 emissions, which has been identified at numerous other forest ecosystems (see e.g. Wohlfahrt
13 et al., 2015; Seco et al., 2015; McKinney et al., 2011).

14 Direct emissions by contrast are intrinsically linked to photosynthesis and are therefore
15 strongly dependent on light as well as temperature. Introducing purely direct emissions of
16 methanol in FORCAST (E-direct) reproduces the observed diurnal profile of both fluxes and
17 concentrations and succeeds in capturing the pronounced daytime peak and sharp drop-off at
18 night seen in both. Modelled mixing ratios, however, peak slightly in advance of the observed
19 maximum (Fig. 6(b); E-direct) and do not drop sharply enough after dusk. Modelled fluxes
20 remain negative at night (Fig. 4(a); E-direct) but are slightly below those observed during the
21 dawn transition period, suggesting that while methanol emissions are light dependent they
22 may not be purely direct emissions (which drop to zero at night), although the limitations of
23 eddy covariance flux measurement techniques at night may introduce error into the
24 observation-model comparison.

25 Combo emissions comprising 80% direct and 20% storage emissions (E-combo) do not
26 reproduce the observed decrease in fluxes and concentrations at night. Modelled nighttime
27 fluxes remain positive and $\sim 0.05\text{--}0.1\text{ mg m}^{-2}\text{ h}^{-1}$ above those observed (Fig. 6(a); E-combo),
28 although as noted above, nighttime flux measurements usually have the greatest uncertainties
29 due to the potential for stable boundary layers and changes in the flux footprint. Additionally,
30 modelled concentrations do not rise sufficiently during the day (with a maximum discrepancy
31 of $\sim 1.5\text{--}2$ ppbv or 15%) nor drop as steeply as observations after dusk (Fig. 4(b); E-combo).
32 Increasing the proportion of direct emissions to 90% (Fig. 4(a) and (b)) improves the fit of



1 both fluxes and concentrations at all times with maximum daytime differences reduced to 0.2
2 $\text{mg m}^{-2} \text{h}^{-1}$ (~30%) and 1.0 ppbv (~8%) respectively. Modelled concentrations still fail to
3 capture the pronounced changes observed at dawn, although this may be the result of
4 boundary layer dilution and canopy flushing. The E-direct simulation gives the best overall
5 model-measurement fit of the emissions sensitivity tests, emphasizing the strong light-
6 dependence of methanol emissions previously noted. Including direct emissions in FORCAsT
7 simulates the bi-directional fluxes and a diel cycle of concentrations similar to those observed
8 at this site although does not fully capture all of the features of the field data at times of
9 transition in particular. However, it should be noted that the fluxes especially represent
10 instantaneous assessments of a situation that rapidly fluctuates in both time and space, which
11 may in part account for the discrepancies between model and measurements. In spite of this
12 caveat, our results indicate that methanol emissions are strongly light-dependent, but that
13 traditional models of primary biogenic emissions (e.g. MEGAN; Guenther et al., 2012) may
14 not fully account for the fundamental processes driving methanol exchange between the
15 canopy and atmosphere even when a small contribution from storage pools (e.g. E-combo90)
16 is included in the model.

17 **3.3.2 Acetaldehyde**

18 Similar to methanol, introducing storage only emissions of acetaldehyde does not capture the
19 peak in fluxes during the day (Fig. 4(c); E-storage), suggesting that acetaldehyde emissions
20 are also light dependent. Modelled concentrations are close to those observed during daylight
21 hours in both magnitude and profile with a maximum difference of ~0.2 ppbv (15%), but do
22 not reproduce the observed drop in concentration just after dusk nor the rapid increase after
23 dawn (Fig. 4(d); E-storage). However, the greater complexity of acetaldehyde production and
24 loss on the timescales involved in canopy-atmosphere exchange makes interpretation of the
25 concentrations more difficult.

26 Introducing purely direct emissions of acetaldehyde (E-direct) has the same effect as for
27 methanol. Fluxes are strongly negative at night in FORCAsT (around 0.01-0.015 $\text{mg m}^{-2} \text{h}^{-1}$
28 below observed fluxes – Fig. 4(c); E-direct) and concentrations rise too quickly during the
29 day, peaking around 4 hours earlier and ~0.10 ppbv (~ 15%) higher than measured mixing
30 ratios (Fig. 4(d); E-direct) with a maximum over-estimation of ~0.15 ppbv (~25%). The steep
31 nighttime drop in observed fluxes and concentrations is reflected (although over-estimated) in
32 the model, but overall the simulations suggest acetaldehyde emissions are not purely direct.



1 In contrast to methanol, acetaldehyde fluxes are reasonably represented by the inclusion of
2 combo emissions comprising 80% direct emissions (Fig. 4(c); E-combo). This captures the
3 diurnal profile of the observations, although not the midday peak, and does not exhibit the
4 same variability in fluxes around dawn and dusk (which may be attributable to the previously
5 described limitations of eddy covariance at these times). Modelled concentrations are within
6 ~ 0.01 ppbv of those observed during daylight hours, and drop quickly after dusk (Fig. 4(d); E-
7 combo). When the proportion of direct emissions is increased to 90%, concentrations peak in
8 the late afternoon when measured mixing ratios decline (Fig. 4(d); E-combo90). The
9 maximum discrepancy is around half that of E-direct and the nighttime decrease in mixing
10 ratios is well captured. Daytime fluxes are similar to those of the E-combo simulation but
11 decrease more sharply in the afternoon and are lower overnight (~ 0.05 mg m⁻² h⁻¹ below
12 observations). None of the simulations captures the observed dip in concentration in the late
13 afternoon. The results suggest that the canopy-atmosphere exchange of acetaldehyde may be
14 best represented using the combination of emissions of traditional emissions models, with the
15 “light-dependent” fraction of 80% as currently suggested (Guenther et al., 2012).

16 **3.4 Effect of stomatal conductance on modelled emissions (S- simulations)**

17 Because direct emissions use only PAR to explain the diurnal cycle of direct emissions (e.g.,
18 the E-direct simulations), here we test the effects of stomatal control on the storage-based
19 emissions mechanism by including stomatal regulation in the storage and combo emissions
20 algorithms. These S- simulations effectively introduce a degree of light-dependence to
21 releases of VOCs from storage pools, although it should be noted that the dependence on PAR
22 introduced in this way is not as strong as for direct emissions. We first present and discuss the
23 results of incorporating stomatal control throughout the day (i.e. the S- simulations using R_{fct}
24 as shown in Eq. 10) for both methanol and acetaldehyde. The effects of modifying the control
25 factor (i.e. the R- simulations using R_{fct} as shown in Eqs. 11a and 11b) are described in
26 Section 3.4.

27 **3.4.1 Methanol**

28 The inclusion of stomatal control of methanol emissions from storage structures into
29 FORCAsT improves the fit of modelled to observed fluxes of methanol for both emissions
30 scenarios that include storage-type emissions (Fig. 6a). For 100% storage emissions, stomatal
31 control (Fig. 6a; S-storage vs. E-storage), daytime fluxes are enhanced and exhibit the



1 pronounced midday peak of the measurements; peak modelled fluxes are now generally <0.2
2 $\text{mg m}^{-2} \text{h}^{-1}$ below those observed. Night-time fluxes are reduced by $\sim 0.1\text{--}0.15 \text{ mg m}^{-2} \text{h}^{-1}$
3 bringing them much closer to observations. However, modelled fluxes are still positive at all
4 times, whereas negative fluxes were measured overnight at the tower. Modelled methanol
5 concentrations now show a slight post-dawn dip followed by a rapid increase, reaching a
6 plateau around 11:00 EST. At this point modelled concentrations diverge from those observed
7 which continue to rise steeply until dusk, peaking nearly 2.5 ppbv ($\sim 25\%$) above modelled
8 levels which rise little during the day. Modelled concentrations continue to remain relatively
9 steady while observed concentrations drop off sharply at night (Fig. 6b; S-storage), indicating
10 a dependence on light that is not adequately represented by including stomatal control.
11 However, some of this behaviour may be a reflection of the discontinuities in modelled
12 stomatal resistance evident at very low values of PAR (Fig. 2a; just after dawn and before
13 dusk). This was tested in a later set of sensitivity experiments in which these discontinuities
14 were smoothed by increasing the level of PAR taken as “daylight”. While this had a
15 substantial effect on modelled R_{stom} in the lower canopy levels following dawn and preceding
16 dusk (Fig. 2h), the impact on R_{ict} and hence simulated emissions was small. The effect on
17 fluxes and concentrations was limited to early morning and late afternoon and was negligible
18 even then (maximum changes of <10% in fluxes and <5% in concentrations at any time; not
19 shown).

20 Modelled fluxes for combo emissions (20% storage emissions) with stomatal control (Fig. 6a;
21 S-combo) mirror those for S-storage although remain slightly higher during the middle of the
22 day and drop a little closer to zero at night. The burst of methanol escaping the canopy just
23 after dusk is less pronounced in S-combo. S-combo fluxes are close to those simulated by
24 increasing the proportion of direct emissions to 90% (E-combo90) apart from the period
25 preceding dusk when stomatal control acts to reduce fluxes sharply. S-combo concentrations
26 of methanol in FORCAsT are also similar to the S-storage simulation but continue to rise
27 until around 16:00 EST at which point they are <0.5 ppbv below measured mixing ratios (Fig.
28 6b; S-combo). However, the diurnal profiles of methanol concentrations simulated by combo
29 emissions without stomatal control (E-combo and E-combo90) is closer to the observed, with
30 90% direct (E-combo90) providing a better overall fit than either of the simulations
31 incorporating stomatal control.



1 3.4.2 Acetaldehyde

2 The effects of including stomatal control of emissions of acetaldehyde from storage pools
3 (Fig. 6c and d) are similar to those described above for methanol. For 100% storage (S-
4 storage vs. E-storage) emissions the diurnal profile of modelled acetaldehyde fluxes is a good
5 fit to observations (Fig. 6c) with a pronounced peak during the middle of the day (~0.005-
6 0.01 mg m⁻² h⁻¹ (maximum 0.03) below measured fluxes) and dropping below zero overnight
7 (again ~0.005-0.01 mg m⁻² h⁻¹ below measurements). Modelled fluxes also show a short-lived
8 dip at ~16:00 EST which does not appear to be seen in the measurements although the high
9 scattering of observations at either end of the day make it difficult to be certain. S-storage
10 modelled concentrations rapidly increase during the day, peaking ~0.15 ppbv (~25%) above
11 those observed and ~4 hours earlier (Fig. 6d). After this peak the model exhibits the night-
12 time decrease in concentrations seen in the observations (Fig. 6d) but still fails to fully
13 reproduce the post-dawn minimum.

14 Model output for the S-combo simulation is almost identical to that for S-storage described
15 above, with the two diverging only at night when the combo emissions are lower reducing
16 fluxes and, to a lesser extent, concentrations of acetaldehyde. Although introducing stomatal
17 control of emissions from storage pools improves the magnitude and diurnal profile of
18 modelled fluxes, particularly for the 100% storage emissions pathway (S-storage),
19 acetaldehyde exchanges at Harvard Forest do not show a strong dependence on stomatal
20 conductance at the canopy scale. Instead they are better represented by the use of traditional
21 emissions models with a proportion of emissions from storage pools and the remainder via
22 direct release (with the best fit given by 80% direct and 20% storage, i.e. E-combo). This is in
23 agreement with the theoretical conclusions reached by Niinemets and Reichstein (2003b) and
24 experimental and field results from Kesselmeier (2001) and Kesselmeier et al. (1997). Jardine
25 et al. (2008) report strong evidence of stomatal control at the leaf and branch level and present
26 field measurements that appear to demonstrate that stomatal regulation is relevant at the
27 ecosystem scale for forests in the USA. Our results do not support this conclusion but the
28 authors also reported large differences in the effect of stomatal aperture between tree species
29 (Jardine et al., 2008) which may help explain the apparent contradiction.



1 **3.5 Threshold stomatal control (R- simulations)**

2 In the R- simulations, the stomatal control function was modified to limit stomatal regulation
3 of storage emissions to transition periods as outlined in Section 2.3.3. This is consistent with
4 laboratory-based observations of transient emissions bursts associated with light-dark
5 transitions. Furthermore, although stomatal regulation at these times may result in changes to
6 emissions later in the day (as the storage pools have built up while emissions were limited by
7 the stomatal aperture (e.g. Jardine et al., 2008)) the traditional emissions algorithms used in
8 FORCAsT were developed from measured dependencies of emissions on light and
9 temperature and can be assumed to capture actual emission rates well during the middle of the
10 day when the stomata are fully open, even if failing to account for the cause. In these
11 simulations, therefore, we effectively assume that there is a point at which the stomatal
12 aperture is sufficient to no longer be a limiting factor. After this point, the stomatal control
13 factor is set to unity to ensure that emissions are no longer dependent on stomatal aperture.
14 Differences between emissions, and therefore (to a lesser extent) fluxes and concentrations,
15 modelled in the R- and E- simulations should therefore be restricted to the periods around
16 dawn and dusk.

17 **3.5.1 Methanol**

18 For 100% storage emissions (R-storage), methanol fluxes show a dip just after dawn and
19 again in the late afternoon, reflecting the period of time when the stomata are partially open
20 (Fig. 7a). At all other times, modelled fluxes match those from the E-storage simulation as
21 expected. Observations do show a drop in methanol fluxes at dawn (~1-2 hours earlier than
22 modelled and greater in magnitude) but not at dusk and are negative overnight. R-storage
23 methanol concentrations match neither the magnitude nor diurnal profile exhibited by the
24 measurements, decreasing during the day as per E-storage but taking longer to recover in the
25 late afternoon (Fig. 7b). The pattern is similar for E- and R-combo emissions with differences
26 between the simulations limited to the transition periods though the effect is less pronounced
27 than the 100% storage case. Fluxes and concentrations are close to those modelled by the E-
28 combo emissions pathway throughout the simulation period, diverging only around dawn and
29 dusk when the stomatal control simulation (R-combo) drops below that without stomatal
30 regulation (E-combo). However, methanol fluxes and concentrations measured above the
31 canopy at Harvard Forest are still most closely matched with the E-direct emissions pathway
32 (Fig. 7a,b).



1 **3.5.2 Acetaldehyde**

2 By contrast, acetaldehyde fluxes for the R-storage simulation show very little change from E-
3 storage until late morning (Fig. 7c). During the middle of the day, R-storage fluxes are nearly
4 double those modelled in E-storage but remain well below those observed. Following a steep
5 decline in fluxes in the afternoon to a minimum just before dusk, the post-dusk spike in fluxes
6 previously noted in the 100% storage emissions simulations is enhanced. Acetaldehyde
7 concentrations for R-storage differ little from E-storage during the day but remain elevated at
8 night (Fig. 7d). Introducing stomatal regulation to combo emissions (R-combo vs. E-combo)
9 has little effect on either fluxes or concentrations with fluxes exhibiting a distinct minimum at
10 dusk (Fig. 7c) and concentrations dropping slightly earlier in the afternoon (Fig. 7d).
11 Observed acetaldehyde fluxes and concentrations are still best reflected with combo
12 emissions and are well captured with the E-combo “traditional” emissions algorithms without
13 explicit parameterisation of stomatal regulation.

14 **3.6 Scaling factor, n**

15 The temporally limited effect of stomatal control in our model simulations is consistent with
16 conclusions drawn from a theoretical study based on results from detailed laboratory
17 experiments (Niinemets and Reichstein, 2003b; Niinemets and Reichstein, 2003a), showing
18 that the stomatal control of biogenic VOC emission rates occur over short timescales. These
19 results suggest that regulation of emissions by stomata occurs over too brief a period to be of
20 significance at an ecosystem scale for highly volatile VOCs. On the other hand, they postulate
21 that emission rates of those VOCs such as methanol that are highly soluble in water and
22 therefore have a high liquid-phase concentration are subject to regulation by stomatal
23 conductance over longer timescales, potentially modifying emissions over scales relevant to
24 other processes involved in canopy-atmosphere exchange. Although this does not appear to be
25 the case at Harvard Forest as the initial introduction of stomatal regulation of emissions into
26 FORCAsT does not modify fluxes over an extended period (Fig. 7), additional simulations
27 were conducted to further explore the hypothesis put forward by Niinemets and Reichstein
28 (2003b). In that analysis the authors concluded that the strength and persistence of stomatal
29 control on leaf-level emissions depended strongly on the solubility of the emitted compound,
30 with more soluble molecules (Henry’s Law coefficient H less than $100 \text{ Pa m}^3 \text{ mol}^{-1}$) more
31 affected. Furthermore they showed that for compounds with H on the order of 10^{-2} - 10^1 Pa m^3



1 mol⁻¹, the degree to which emissions were influenced by the stomata scaled with H . Both
2 acetaldehyde and methanol have solubilities in this range. Hence in the final stomatal control
3 simulations (R-storageN15, R-storageN6, R-comboN15 and R-combo6) we scaled the
4 “degree” of regulation by altering the scaling factor, n , in Eqs. 11a and 11b (see Table 5). In
5 addition to scaling R_{fet} this also alters the duration of stomatal control (i.e. the time taken for
6 R_{fet} in Eq. 10 to reach values over 1.0) as shown in Fig. 2. Reducing n reduces the time over
7 which stomatal control regulates emissions (Fig. 2d and e). Doubling n increases the duration
8 of stomatal control to such an extent that emissions from the lower canopy levels are limited
9 by the stomata throughout the day (Fig. 2f and g).

10 In the case of methanol, changing n makes little difference to simulated daytime fluxes (Fig.
11 7a; R-storageN6 and R-comboN6). However, night-time fluxes were enhanced slightly
12 (~ 0.02 mg m⁻² h⁻¹ for 100% storage emissions and ~ 0.01 mg m⁻² h⁻¹ for 80% storage
13 emissions) when n was doubled. Night-time concentrations (Fig. 7b) also increased slightly
14 around dawn particularly for R-storageN6 (~ 0.4 ppbv above R-storage mixing ratios). In
15 contrast, concentrations at Harvard Forest were observed to fall sharply in the early morning.
16 Modelled mixing ratios were reduced slightly throughout the day when n was increased in
17 both storage and combo simulations (R-storageN6 and R-comboN6) with strong decreases
18 followed by rapid recovery in the late afternoon. Changes at all times were negligible when n
19 was reduced to 1.5 (not shown).

20 The effects on acetaldehyde concentrations and fluxes are similar, with increases in both at
21 night when n is increased to 6, although acetaldehyde fluxes are also slightly enhanced during
22 the middle of the day (~ 0.002 mg m⁻² h⁻¹ for both R-storageN6 and R-comboN6; Fig. 7c).
23 Changes in daytime concentrations are limited to the times around dawn and dusk (Fig. 7d).
24 Halving n also has little effect on acetaldehyde (not shown).

25 These results are consistent with observations of canopy structure at Harvard Forest; foliage is
26 densest in the upper canopy. Fig. 2 shows that changing n has the biggest impact on the lower
27 canopy levels where light is limited, foliage biomass is low (over 50% of the biomass is found
28 in the top 20% of the canopy at Harvard Forest; Parker (1998)) and emission rates small.

29 Our simulations again suggest that the complexity of the competing in-canopy processes act
30 to buffer the stomatal control of emissions observed at the leaf and branch level. Stomatal
31 aperture appears to affect emissions over too short a timescale to be observable at the canopy
32 scale when other sources and sinks are fully accounted for. The times around dawn and dusk



1 are also associated with rapid changes in chemistry and atmospheric dynamics, which likely
2 outweigh the small differences in emission rates due to stomatal control. Our findings indicate
3 that the inclusion of a “light-dependent fraction” in current emissions algorithms capture the
4 changes in storage emissions due to changes in stomatal aperture sufficiently well at the
5 canopy-scale.

6 **4 Conclusions**

7 When light-dependent emissions of methanol and acetaldehyde were included, the FORCAsT
8 canopy-atmosphere exchange model successfully simulated the bi-directional exchange of
9 methanol and acetaldehyde at Harvard Forest, a northern mid-latitude mixed deciduous
10 woodland. The light-dependence of both methanol and acetaldehyde emissions at the leaf-
11 level has been ascribed to the stomatal control of diffusion from storage pools, which would
12 otherwise be expected to be dependent on temperature alone. We incorporated a simple
13 parameterisation of the regulation of emissions according to stomatal aperture into FORCAsT
14 to determine how stomatal control affects canopy-top fluxes and concentrations of methanol
15 and acetaldehyde at this site.

16 We found that although some simulations that included stomatal regulation of emissions
17 showed a good fit to measured fluxes, none proved effective in reproducing both the observed
18 concentrations and fluxes. Instead, our simulations show that the algorithms currently used for
19 modelling foliage emissions of oVOC are capable of capturing fluxes and concentrations of
20 both methanol and acetaldehyde near the top of the canopy and are therefore appropriate for
21 use at the ecosystem-scale. Our results demonstrate that canopy-top fluxes of methanol and
22 acetaldehyde are determined primarily by the relative strengths of foliage emissions and dry
23 deposition indicating that 3-D atmospheric chemistry and transport models must include a
24 treatment of deposition that is not only dynamically intrinsically linked to land surface
25 processes but is consistent with the emissions scheme.

26 Our results show that it is possible to model canopy top fluxes of methanol and acetaldehyde,
27 and to capture bi-directional exchange without the need for including direct representations of
28 stomatal control of emissions. Overall, we find that the bi-directional exchange of methanol at
29 Harvard Forest is best modelled with traditional emissions models (e.g. MEGAN; Guenther et
30 al. 2012) assuming 100% light-dependent (direct) emissions. In the case of acetaldehyde,
31 modelled concentrations prove robust with a relatively good fit to observations for all
32 emissions scenarios employed here, likely due to the greater number of chemical sources and



1 sinks of acetaldehyde in comparison to methanol. Canopy-top acetaldehyde fluxes at this site
2 are also best modelled with emissions algorithms that include light dependence directly (i.e.
3 without the introduction of stomatal control). In contrast to methanol, however, acetaldehyde
4 emissions at Harvard Forest appear to be derived from both direct synthesis and storage pools,
5 with 80% direct emissions giving the best overall fit.

6 Given that observed methanol fluxes appear strongly correlated with stomatal conductance at
7 small stomatal apertures it is perhaps surprising that we found no evidence supporting the
8 suggestion that stomatal control of methanol emissions are observable at the canopy scale. It
9 is likely therefore that this correlation is ascribable to the strong dependence of methanol
10 deposition on stomatal resistance.

11 Our results highlight the importance of the holistic treatment and coupling between land
12 surface sources and sinks. The use of explicit and consistent dynamic representations of
13 emissions and deposition, which dominate the in-canopy budgets for these longer-lived
14 oVOC, are needed in atmospheric chemistry and transport models. Such an approach would
15 adequately account for the role of the stomata in both processes and allow bi-directional
16 exchange to be successfully simulated without the need for including either leaf-level process
17 detail or a compensation point.

18 However, this study also demonstrates the need for a better understanding and representation
19 of the complex relationship between turbulence, fluxes and concentration gradients within and
20 above the forest canopy. Such understanding can only be achieved through further modelling
21 studies at a range of scales in combination with robust measurements of concentrations and
22 fluxes of VOCs, their primary oxidants and oxidation products at multiple heights within the
23 forest canopy.

24 **Acknowledgements**

25 This material is based upon work supported by the National Science Foundation under Grant
26 No. AGS 1242203.

27



1 **References**

- 2 Ashworth, K, S H Chung, R J Griffin, J Chen, R Forkel, A M Bryan, and A L Steiner. 2015.
3 “FORest Canopy Atmosphere Transfer (FORCAsT) 1.0: a 1-D Model of Biosphere–
4 Atmosphere Chemical Exchange.” *Geoscientific Model Development* 8 (11): 3765–84.
5 doi:10.5194/gmd-8-3765-2015-supplement.
- 6 Baldocchi, D D, B B Hicks, and P Camara. 1987: A canopy stomatal resistance model for
7 gaseous deposition to vegetated surfaces." *Atmospheric Environment* 21 (1), 91-101.
- 8 Bryan, A M, S B Bertman, M A Carroll, S Dusanter, G D Edwards, R Forkel, S Griffith, et al.
9 2012. “In-Canopy Gas-Phase Chemistry During CABINEX 2009: Sensitivity of a 1-D
10 Canopy Model to Vertical Mixing and Isoprene Chemistry.” *Atmospheric Chemistry and*
11 *Physics* 12 (18): 8829–49. doi:10.5194/acp-12-8829-2012-supplement.
- 12 Bryan, Alexander M., Susan J. Cheng, Kirsti Ashworth, Alex B. Guenther, Brady S.
13 Hardiman, Gil Bohrer, and Allison L. Steiner: Forest-atmosphere BVOC exchange in diverse
14 and structurally complex canopies: 1-D modeling of a mid-successional forest in northern
15 Michigan, *Atmos. Environ.*, 120, 217-226, 2015., doi: 10.1016/j.atmosenv.2015.08.094.
- 16 Butler, T. M., Taraborrelli, D., Brühl, C., Fischer, H., Harder, H., Martinez, M., Williams, J.,
17 Lawrence, M. G., and Lelieveld, J.: Improved simulation of isoprene oxidation chemistry with
18 the ECHAM5/MESSy chemistry-climate model: lessons from the GABRIEL airborne field
19 campaign, *Atmos. Chem. Phys.*, 8, 4529-4546, doi:10.5194/acp-8-4529-2008, 2008.
- 20 Chen, Jianjun, and Robert J Griffin. 2005. “Modeling Secondary Organic Aerosol Formation
21 From Oxidation of α -Pinene, B-Pinene, and D-Limonene.” *Atmospheric Environment* 39 (40):
22 7731–44. doi:10.1016/j.atmosenv.2005.05.049.
- 23 Environmental Protection Agency (EPA), 2015, National and Regional Air Quality Trends.
24 Available on-line at <http://www3.epa.gov/airtrends/aqtrends.html>
- 25 Fall, Ray, and Andrew Benson. 1996. “Leaf Methanol- the Simplest Natural Product From
26 Plants.” *Trends in Plant Science* 1 (9): 296–301. doi:10.1016/S1360-1385(96)88175-0.
- 27 Fischer, E V, D J Jacob, R M Yantosca, M P Sulprizio, D B Millet, J Mao, F Paulot, et al.
28 2014. “Atmospheric Peroxyacetyl Nitrate (PAN): a Global Budget and Source Attribution.”
29 *Atmospheric Chemistry and Physics* 14 (5): 2679–98. doi:10.5194/acp-14-2679-2014-
30 supplement.



- 1 Folberth, G A, D A Hauglustaine, J Lathiere, and F Brocheton. 2006. “Interactive Chemistry
2 in the Laboratoire De Météorologie Dynamique General Circulation Model: Model
3 Description and Impact Analysis of Biogenic Hydrocarbons on Tropospheric Chemistry.”
4 *Atmospheric Chemistry and Physics* 6 (June): 2273–2319. doi:10.5194/acp-6-2273-2006.
- 5 Ganzeveld, L., Eerdekens, G., Feig, G., Fischer, H., Harder, H., Königstedt, R., Kubistin, D.,
6 Martinez, M., Meixner, F. X., Scheeren, H. A., Sinha, V., Taraborrelli, D., Williams, J., Vilà-
7 Guerau de Arellano, J., and Lelieveld, J.: Surface and boundary layer exchanges of volatile
8 organic compounds, nitrogen oxides and ozone during the GABRIEL campaign, Atmos.
9 Chem. Phys., 8, 6223-6243, doi:10.5194/acp-8-6223-2008, 2008.
- 10 Gao, W, M L Wesely, and P V Doskey. 1993. “Numerical Modeling of the Turbulent
11 Diffusion and Chemistry of NO_x, O₃, Isoprene, and Other Reactive Trace Gases in and Above
12 a Forest Canopy.” *Journal of Geophysical Research* 98 (D10): 18339–53.
- 13 Geron, Chris, Rei Rasmussen, Robert R Arnts, and Alex Guenther. 2000. “A Review and
14 Synthesis of Monoterpene Speciation From Forests in the United States.” *Atmospheric*
15 *Environment* 34 (February): 1761–81.
- 16 Goldstein, A H, S C Wofsy, and C M Spivakovsky. 1995. “Seasonal Variations of
17 Nonmethane Hydrocarbons in Rural New England: Constraints on OH Concentrations in
18 Northern Midlatitudes.” *Journal of Geophysical Research* 100 (D10): 21023–33.
19 doi:10.1029/95JD02034.
- 20 Goulden, M.L., J.W. Munger, S.M. Fan, B.C. Daube, and S.C. Wofsy: Measurements of
21 carbon sequestration by long-term eddy covariance: methods and a critical evaluation of
22 accuracy, *Global Change Biol.*, 2, 169–182, 1996.
- 23 Graus, M., Müller, M., and Hansel, A.: High resolution PTRTOF: quantification and formula
24 confirmation of VOC in real time, *J. Am. Soc. Mass. Spectr.*, 21, 1037–1044,
25 doi:10.1016/j.jasms.2010.02.006, 2010.
- 26 Griffin, Robert J, Donald Dabdub, and John H Seinfeld 2002. “Secondary Organic Aerosol 1.
27 Atmospheric Chemical Mechanism for Production of Molecular Constituents.” *Journal of*
28 *Geophysical Research* 107 (D17): 4332. doi:10.1029/2001JD000541.
- 29 Griffin, Robert J, Donald Dabdub, and John H Seinfeld. 2005. “Development and Initial
30 Evaluation of a Dynamic Species-Resolved Model for Gas Phase Chemistry and Size-



- 1 Resolved Gas/Particle Partitioning Associated with Secondary Organic Aerosol Formation.”
2 *Journal of Geophysical Research* 110 (D5): D05304. doi:10.1029/2004JD005219.
- 3 Grote, R, and U Niinemets. 2008. “Modeling Volatile Isoprenoid Emissions - a Story with
4 Split Ends.” *Plant Biology* 10 (1): 8–28. doi:10.1055/s-2007-964975.
- 5 Gu, Lianhong, Eva M. Falge, Tom Boden, Dennis D. Baldocchi, T.A. Black, Scott R. Saleska,
6 Tanja Suni, Shashi B. Verma, Timo Vesala, Steve C. Wofsy, Liukang Xu, Objective threshold
7 determination for nighttime eddy flux filtering, *Agricultural and Forest Meteorology*, 128, (3–
8 4), 179-197, 2005. doi: 10.1016/j.agrformet.2004.11.006
- 9 Guenther, A B, X Jiang, C L Heald, T Sakulyanontvittaya, T Duhl, L K Emmons, and X
10 Wang. 2012. “The Model of Emissions of Gases and Aerosols From Nature Version 2.1
11 (MEGAN2.1): an Extended and Updated Framework for Modeling Biogenic Emissions.”
12 *Geoscientific Model Development* 5 (6): 1471–92. doi:10.5194/gmd-5-1471-2012.
- 13 Guenther, A.B., Zimmerman, P.R., Harley, P.C., Monson, R.K., and Fall, R., J., 1993:
14 *Geophys. Res.*, 98 (D7), 12609-12617, doi: 10.1029/93JD00527.
- 15 Harley, P., Greenberg, J., Niinemets, Ü., and Guenther, A.: Environmental controls over
16 methanol emission from leaves, *Biogeosciences*, 4, 1083-1099, doi:10.5194/bg-4-1083-2007,
17 2007
- 18 Heikes, Brian G, Wonil Chang, Michael E Q Pilson, Elijah Swift, Hanwant B Singh, Alex
19 Guenther, Daniel J Jacob, et al. 2002. “Atmospheric Methanol Budget and Ocean
20 Implication.” *Global Biogeochemical Cycles* 16 (4): 80–1–80–13.
21 doi:10.1029/2002GB001895.
- 22 Helmig, Detlev, Lee F Klinger, Alex Guenther, Peter Harley, Chris Geron, and Patrick
23 Zimmerman. 1999. “Biogenic Volatile Organic Compound Emissions (BVOCs) 1.
24 Identifications From Three Continental Sites in the U.S.” *Chemosphere* 38 (9): 2163–87.
- 25 Huve, K, M Christ, E Kleist, R Uerlings, U Niinemets, A Walter, and J Wildt. 2007.
26 “Simultaneous Growth and Emission Measurements Demonstrate an Interactive Control of
27 Methanol Release by Leaf Expansion and Stomata.” *Journal of Experimental Botany* 58 (7):
28 1783–93. doi:10.1093/jxb/erm038.



- 1 Jacob, Daniel J, Brendan D Field, Emily M Jin, Isabelle Bey, Qinbin Li, Jennifer A Logan,
2 and Robert M Yantosca. 2002. "Atmospheric Budget of Acetone." *Journal of Geophysical*
3 *Research* 107 (D10). doi:10.1029/2001JD000694.
- 4 Jardine, K, P Harley, T Karl, A Guenther, M Lerdau, and J E Mak. 2008. "Plant Physiological
5 and Environmental Controls Over the Exchange of Acetaldehyde Between Forest Canopies
6 and the Atmosphere." *Biogeosciences* 5 (November): 1559–72. doi:10.5194/bg-5-1559-2008.
- 7 Jarvis, P G. 1976. "The interpretation of the variations in leaf water potential and stomatal
8 conductance found in canopies in the field. *Phil. Trans. R. Soc. London B.* 273, 593-610
- 9 Jarvis, P G, J.M. Massheder, S.E. Hale, J.B. Moncrieff, M. Rayment, and S.L. Scott: Seasonal
10 variation of carbon dioxide, water vapor, and energy exchanges of a boreal black spruce
11 forest, *J. Geophys. Res. Atmospheres*, 102 (D24), 28953–28966, 1997. doi:
12 10.1029/97JD01176
- 13 Jordan, A., Haidacher, S., Hanel, G., Hartungen, E., Herbig, J., Märk, L., Schottkowsky, R.,
14 Seehauser, H., Sulzer, P., and Märk, T. D.: An online ultra-high sensitivity proton-transfer-
15 reaction mass-spectrometer combined with switchable reagent ion capability (PTR + SRI -
16 MS), *Int. J. Mass. Spectrom.*, 286, 32–38, doi:10.1016/j.ijms.2009.06.006, 2009a.
- 17 Jordan, A., Haidacher, S., Hanel, G., Hartungen, E., Märk, L., Seehauser, H., Schottkowsky,
18 R., Sulzer, P., and Märk, T. D.: A high resolution and high sensitivity proton-transfer-reaction
19 time-of flight mass spectrometer (PTR-TOF-MS), *Int. J. Mass. Spectrom.*, 286, 122–128,
20 doi:10.1016/j.ijms.2009.07.005, 2009b.
- 21 Karl, T, A Guenther, C Spirig, A Hansel, and R Fall. 2003. "Seasonal Variation of Biogenic
22 VOC Emissions Above a Mixed Hardwood Forest in Northern Michigan." *Geophysical*
23 *Research Letters* 30 (23): 2186. doi:10.1029/2003GL018432.
- 24 Karl, T, A J Curtis, T N Rosenstiel, R K Monson, and R Fall. 2002. "Transient Releases of
25 Acetaldehyde From Tree Leaves - Products of a Pyruvate Overflow Mechanism?." *Plant, Cell*
26 *& Environment* 25 (August): 1121–31. doi:10.1046/j.0016-8025.2002.00889.x.
- 27 Karl, T, P Harley, A Guenther, R Rasmussen, B Baker, K Jardine, and E Nemitz. 2005. "The
28 Bi-Directional Exchange of Oxygenated VOCs Between a Loblolly Pine (*Pinus Taeda*)
29 Plantation and the Atmosphere." *Atmospheric Chemistry and Physics* 5 (November): 3015–
30 31.



- 1 Karl, T, P Harley, L Emmons, B Thornton, A Guenther, C Basu, A Turnipseed, and K
2 Jardine. 2010. "Efficient Atmospheric Cleansing of Oxidized Organic Trace Gases by
3 Vegetation, *Science*, 330 (6005), 816-819, doi:10.1126/science.1192534
- 4 Kesselmeier, J. 2001. "Exchange of short-chain oxygenated volatile organic compounds
5 (VOCs) between plants and the atmosphere: A compilation of field and laboratory studies, J.
6 *Atmos. Chem.*, 29, 219-233, 2001.
- 7 Kesselmeier, J., Bode, K., Hoffman, U., Muller, H., Schaffer, L., Wolf, A., Ciccioli, P.,
8 Brancaleoni, E., Cecinato, A., Frattoni, M., Foster, P., Ferrari, C., Jacob, V., Fugit, J. L.,
9 Dutaur, L., Simon, V., and Torres, L.: Emission of short chained organic acids, aldehydes,
10 monoterpenes from *Quercus Ilex L.* and *Pinus pinea L.* in relation to physiological activities,
11 carbon budget and emission algorithms, *Atmos. Environ.*, 31, 119-133, 1997.
- 12 Kreuzwieser, Jürgen, Frank Kühnemann, Albert Martis, Heinz Rennenberg, and Wolfgang
13 Urban. 2000. "Diurnal Pattern of Acetaldehyde Emission by Flooded Poplar Trees."
14 *Physiologia Plantarum* 108: 79–86. doi:10.1034/j.1399-3054.2000.108001079.x.
- 15 McKinney, K A, B H Lee, A Vasta, T V Pho, and J W Munger. 2011. "Emissions of
16 Isoprenoids and Oxygenated Biogenic Volatile Organic Compounds From a New England
17 Mixed Forest." *Atmospheric Chemistry and Physics* 11 (10): 4807–31. doi:10.5194/acp-11-
18 4807-2011.
- 19 Millet, D B, A Guenther, D A Siegel, N B Nelson, H B Singh, J A de Gouw, C Warneke, et
20 al. 2010. "Global Atmospheric Budget of Acetaldehyde: 3-D Model Analysis and Constraints
21 From in-Situ and Satellite Observations." *Atmospheric Chemistry and Physics* 10 (7): 3405–
22 25. doi:10.5194/acp-10-3405-2010.
- 23 Millet, D B, M J Mohr, K C Wells, T J Griffis, and D Helmig. 2011. "Sources and
24 Seasonality of Atmospheric Methanol Based on Tall Tower Measurements in the US Upper
25 Midwest." *Atmospheric Chemistry and Physics* 11 (21): 11145–56. doi:10.5194/acp-11-
26 11145-2011.
- 27 Moody, J L, J W Munger, A H Goldstein, D J Jacob, and S C Wofsy. 1998. "Harvard Forest
28 Regional-Scale Air Mass Composition by Patterns in Atmospheric Transport History
29 (PATH)." *Journal of Geophysical Research* 103 (D11): 13181–94. doi:10.1029/98JD00526.
- 30 Müller, M., Graus, M., Ruuskanen, T. M., Schnitzhofer, R., Bamberger, I., Kaser, L.,
31 Titzmann, T., Hörtnagl, L., Wohlfahrt, G., Karl, T., and Hansel, A.: First eddy covariance flux



- 1 measurements by PTR-TOF, *Atmos. Meas. Tech.*, 3, 387-395, doi:10.5194/amt-3-387-2010,
2 2010.
- 3 Munger, J William, Steven C Wofsy, Peter S Bakwin, Song-Miao Fan, Michael L Goulden,
4 Bruce C Daube, Allen H Goldstein, Kathleen E Moore, and David R Fitzjarrald. 1996.
5 “Atmospheric Deposition of Reactive Nitrogen Oxides and Ozone in a Temperate Deciduous
6 Forest and a Subarctic Woodland: 1. Measurements and Mechanisms.” *Journal of*
7 *Geophysical Research* 101 (D7): 12639–57. doi:10.1029/96JD00230.
- 8 Munger W, and Wofsy S. 1999a. Canopy-Atmosphere Exchange of Carbon, Water and
9 Energy at Harvard Forest EMS Tower since 1991. *Harvard Forest Data Archive: HF004*.
10 Data available at:
11 <http://harvardforest.fas.harvard.edu:8080/exist/apps/datasets/showData.html?id=hf004>
- 12 Munger W, and Wofsy S. 1999b. Concentrations and Surface Exchange of Air Pollutants at
13 Harvard Forest EMS Tower since 1990. *Harvard Forest Data Archive: HF066*. Data
14 available at:
15 <http://harvardforest.fas.harvard.edu:8080/exist/apps/datasets/showData.html?id=hf066>
- 16 Munger W, and Wofsy S. 1999c. Biomass Inventories at Harvard Forest EMS Tower since
17 1993 *Harvard Forest Data Archive: HF069*. Data available at:
18 <http://harvardforest.fas.harvard.edu:8080/exist/apps/datasets/showData.html?id=hf069>
- 19 Nemecek-Marshall, Michele, Robert C MacDonald, Jennifer J Franzen, Cheryl L
20 Wojciechowski, and Ray Fall. 1995. “Methanol Emission From Leaves: Enzymatic Detection
21 of Gas-Phase Methanol and Relation of Methanol Fluxes to Stomatal Conductance and Leaf
22 Development.” *Plant Physiology* 108 (4): 1359–68.
- 23 Niinemets, Ülo, and Markus Reichstein. 2003a. “Controls on the Emission of Plant Volatiles
24 Through Stomata: a Sensitivity Analysis.” *Journal of Geophysical Research* 108 (D7): 4211.
25 doi:10.1029/2002JD002626.
- 26 Niinemets, Ülo, and Markus Reichstein. 2003b. “Controls on the Emission of Plant Volatiles
27 Through Stomata: Differential Sensitivity of Emission Rates to Stomatal Closure Explained.”
28 *Journal of Geophysical Research* 108 (D7): 4208. doi:10.1029/2002JD002620.
- 29 Niinemets, Ülo, Francesco Loreto, and Markus Reichstein. 2004. “Physiological and
30 Physicochemical Controls on Foliar Volatile Organic Compound Emissions.” *Trends in Plant*
31 *Science* 9 (4): 180–86. doi:10.1016/j.tplants.2004.02.006.



- 1 F. M. O'Connor, C. E. Johnson, O. Morgenstern, N. L. Abraham, P. Braesicke, M. Dalvi, G.
2 A. Folberth, M. G. Sanderson, P. J. Telford, A. Voulgarakis, P. J. Young, G. Zeng, W. J.
3 Collins, and J. A. Pyle: Evaluation of the new UKCA climate-composition model – Part 2:
4 The Troposphere, *Geosci. Model Dev.*, 7, 41-91, 2014. doi:10.5194/gmd-7-41-2014
- 5 Park, J H, A H Goldstein, J Timkovsky, S Fares, R Weber, J Karlik, and R Holzinger. 2013.
6 “Active Atmosphere-Ecosystem Exchange of the Vast Majority of Detected Volatile Organic
7 Compounds.” *Science* 341 (6146): 643–47. doi:10.1126/science.1235053.
- 8 Parker, G G. 1998. "Light Transmittance in a Northeastern Mixed Hardwood Canopy",
9 *Smithsonian Environmental Research Center Technical Report*.
- 10 Sander, R. 1999. "Compilation of Henry's Law Constants for Inorganic and Organic Species
11 of Potential Importance in Environmental Chemistry". Available at: [http://www.henrys-](http://www.henrys-law.org/henry-3.0.pdf)
12 [law.org/henry-3.0.pdf](http://www.henrys-law.org/henry-3.0.pdf)
- 13 Seco, Roger, Josep Peñuelas, and Iolanda Filella. 2007. “Short-Chain Oxygenated VOCs:
14 Emission and Uptake by Plants and Atmospheric Sources, Sinks, and Concentrations.”
15 *Atmospheric Environment* 41 (12): 2477–99. doi:10.1016/j.atmosenv.2006.11.029.
- 16 Seco, Roger, Thomas Karl, Alex Guenther, Kevin P Hosman, Stephen G Pallardy, Lianhong
17 Gu, Chris Geron, Peter Harley, and Saewung Kim. 2015. “Ecosystem-Scale Volatile Organic
18 Compound Fluxes During an Extreme Drought in a Broadleaf Temperate Forest of the
19 Missouri Ozarks (Central USA).” *Global Change Biology* 21 (10): 3657–74.
20 doi:10.1111/gcb.12980.
- 21 Shuttleworth, W J, J H C Gash, C R Lloyd, C J Moore, J Roberts, A D Marques, G Fisch, V
22 D Silva, M D G Ribeiro, L C B Molion, L D D Sa, J C A Nobre, O M R Cabral, S R Patel,
23 and J C Demoraes. 1984. “Eddy-Correlation Measurements of Energy Partition for
24 Amazonian Forest”, *Quarterly Journal Of The Royal Meteorological Society*, 110 (466),
25 1143-1162. doi: 10.1002/qj.49711046622
- 26 Singh, Hanwant B, M Kanakidou, P J Crutzen, and D J Jacob. 1995. “High Concentrations
27 and Photochemical Fate of Oxygenated Hydrocarbons in the Global Troposphere.” *Nature*
28 378 (November): 50–54. doi:10.1038/378050a0.
- 29 Stavrakou, T, A Guenther, A Razavi, L Clarisse, C Clerbaux, P F Coheur, D Hurtmans, et al.
30 2011. “First Space-Based Derivation of the Global Atmospheric Methanol Emission Fluxes.”
31 *Atmospheric Chemistry and Physics* 11 (10): 4873–98. doi:10.5194/acp-11-4873-2011.



- 1 Steiner, A. L., Pressley, S. N., Botros, A., Jones, E., Chung, S. H., and Edburg, S. L.: Analysis
2 of coherent structures and atmosphere-canopy coupling strength during the CABINEX field
3 campaign, *Atmos. Chem. Phys.*, 11, 11921-11936, doi:10.5194/acp-11-11921-2011, 2011.
- 4 Tie, Xuexi, Alex Guenther, and Elisabeth Holland. 2003. "Biogenic Methanol and Its Impacts
5 on Tropospheric Oxidants." *Geophysical Research Letters* 30 (17): 1881.
6 doi:10.1029/2003GL017167.
- 7 Wesely, M L. 1989. "Parameterization of Surface Resistances to Gaseous Dry Deposition in
8 Regional-Scale Numerical-Models." *Atmospheric Environment* 23 (6): 1293-1304.
9 doi:10.1016/0004-6981(89)90153-4.
- 10 Wohlfahrt, G, C Amelynck, C Ammann, A Arneth, I Bamberger, A H Goldstein, L Gu, et al.
11 2015. "An Ecosystem-Scale Perspective of the Net Land Methanol Flux: Synthesis of
12 Micrometeorological Flux Measurements." *Atmospheric Chemistry and Physics* 15 (13):
13 7413-27. doi:10.5194/acp-15-7413-2015-supplement.

14



- 1 Table 1. Atmospheric and meteorological measurements relevant to this study made between
 2 7th June and 24th September 2012 at the EMS Tower in Harvard Forest.

Type	Measurement	Height (m)	Instrument
Chemical			
Methanol, CH ₃ OH ^a	Concentration, Flux	29	PTR-TOF-MS, Iconicon Analytik
Acetaldehyde, CH ₃ CHO ^a	Concentration, Flux	29	PTR-TOF-MS, Iconicon Analytik
CO ^b	Concentration	29	Modified IR-absorption gas-filter correlation analyser
O ₃ ^b	Concentration	29, 24.1, 18.3, 12.7, 7.5, 4.5, 0.8, 0.3	UV absorbance instrument
Water Vapour ^c	Concentration	29	Licor CO ₂ -H ₂ O sensor
Meteorological			
Air temperature ^c		29, 27.9, 22.6, 15.4, 7.6, 2.5	30kW precision thermistor in aspirated radiation shield
PAR ^c		29, 12.7	Quantum sensor
Windspeed ^c	Horizontal, vertical	29	AT1 sonic anemometer
Wind direction ^c		29	AT1 sonic anemometer
Relative humidity ^c		29, 22.6, 15.4, 7.6, 2.5	Thin film capacitor sensor in aspirated radiation shield

- 3 ^adata provided by McKinney and Liu; ^bMunger and Wofsy (1999b); ^cMunger and Wofsy (1999a)

- 4 Table 2. Boundary and initial conditions used for the FORCAST simulations.

Model parameter or variable	Value
Total leaf area index (m ² leaf area m ⁻² ground area) ^a	3.67
Average canopy height (m) ^b	23.0



Average trunk height (m) ^b	6.0
Meteorology (values measured at 29 m)	
Air temperature (°C) ^c	20.9
Wind speed (m s ⁻¹) ^c	1.589
Friction velocity, u* (m s ⁻¹) ^d	0.278
Standard deviation of vertical wind velocity, σ_w (m s ⁻¹) ^d	0.351
Concentrations at 29 m (ppbv)	
Isoprene ^e	0.939
Total monoterpenes ^e	0.449
MVK-MCR ^e	0.786
Methanol ^e	10.11
Acetaldehyde ^e	0.620
Acetone ^e	2.608
Ozone ^f	33.54
CO ^f	164.8
Water vapour ^c	1.861%
Miscellaneous	
Ozone at ground-level (0.3 m) ^f	20.35 ppbv
Temperature at ground-level (2.5 m) ^c	18.1 °C
Soil Temperature at 15, 40, 50 and 90 cm depth ^a	24.9, 25.9, 25.9, 21.4 °C
Soil Moisture at 15, 40, 50 and 90 cm depth ^a	0.18, 0.15, 0.17, 0.18
NO ₂ at 29 m ^g	1.00 ppbv
N ₂ O ₅ at 29 m ^g	1.50 ppbv



1 ^aMunger and Wofsy (1999c); ^bParker (1998); ^cMunger and Wofsy (1999a); ^ddata provided by Munger; ^edata
 2 provided by McKinney and Liu; ^fMunger and Wofsy (1999b); ^gMoody et al. (1998)

3 Table 3. Deposition parameters for methanol and acetaldehyde.

Chemical	Henry's Law constant	Diffusivity	Reactivity factor
Methanol	2.2E02 ^a	1.33 ^b	1.0 ^c
ALD1 (acetaldehyde) ^d	11.4	1.6	1.0

4 ^aSander (1999); ^bWesely (1989); ^cKarl et al. (2010); ^dAshworth et al. (2015)

5 Table 4. Values of stomatal resistance coefficients and parameters used in FORCAsT.

Coefficient	Value
r_{smin}	90.0
b_{rs}	200.0
T_{min}	-2.0
T_{max}	45.0
T_0	30.0
b_v	0.5
a	0.066667
b_ϕ	1.666667

6 Table 5. Modifications to the base case for each of the sensitivity simulations.

Simulation	Changes from baseline simulation
Emissions (E) of methanol and acetaldehyde included as:	
E-direct	100% direct emissions
E-storage	100% storage emissions
E-combo	80% direct; 20% storage
E-combo90	90% direct; 10% storage
Stomatal control (S) of storage emissions included:	
S-storage	Activity factor, γ_T , for storage emissions scaled by stomatal control factor,



	R_{fct} (Eqs. 2 and 9, with $n=3$)
S-combo	Activity factor, γ_r , for storage emissions scaled by stomatal control factor, R_{fct} (Eqs. 9 and 10, with $n=3$); 80% direct and 20% storage
Stomatal control of storage emissions using modified stomatal control factor, R_{fct} (R):	
R-storage	Threshold stomatal control factor used (Eq. 11)
R-storageP	Threshold stomatal control factor used (Eq. 11) and daytime threshold for PAR increased to 10.0
R-storageN15	Threshold stomatal control factor used (Eq. 11) with scaling factor n set to 1.5
R-storageN6	Threshold stomatal control factor used (Eq. 11) with scaling factor n set to 6.0
R-combo	Threshold stomatal control factor used (Eq. 11); 80% direct and 20% storage
R-comboP	Threshold stomatal control factor used (Eq. 11) and daytime threshold for PAR increased to 10.0; 80% direct and 20% storage
R-comboN15	Threshold stomatal control factor used (Eq. 11) with scaling factor n set to 1.5; 80% direct and 20% storage
R-comboN6	Threshold stomatal control factor used (Eq. 11) with scaling factor n set to 6.0; 80% direct and 20% storage

- 1 Table 6a. Emission factors (nmol m^{-2} (projected leaf area) s^{-1}) for VOCs included in
- 2 FORCAsT baseline simulation.

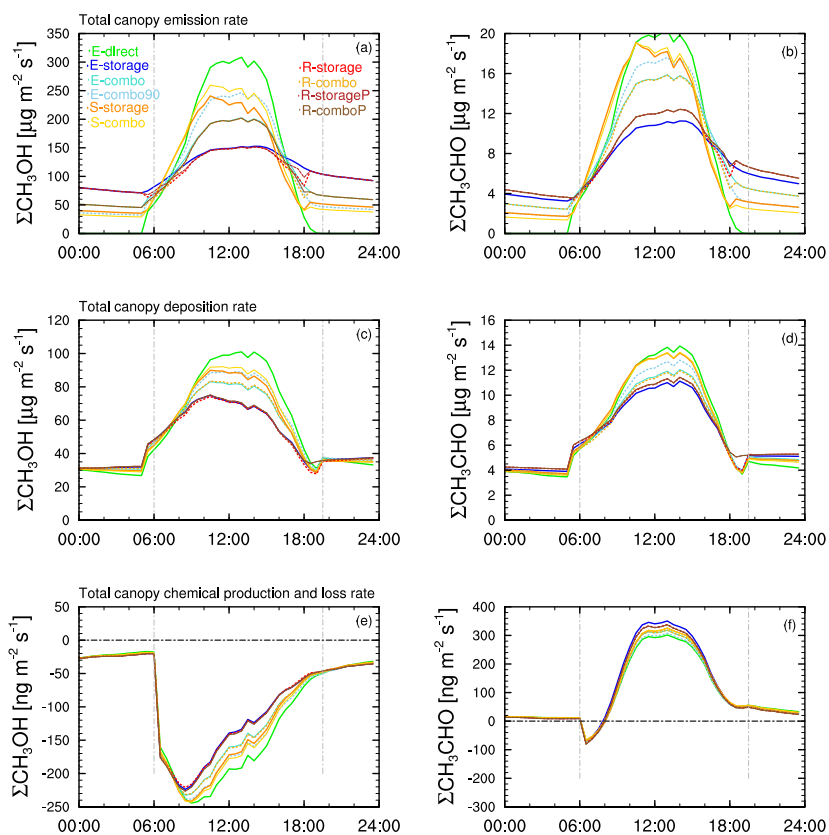
VOC	Direct	Storage
Isoprene	4.83 ^a	0.000
α -pinene	0.000	0.071 ^b
β -pinene	0.000	0.032 ^b
<i>d</i> -limonene	0.000	0.054 ^b
Methanol	0.000	0.000



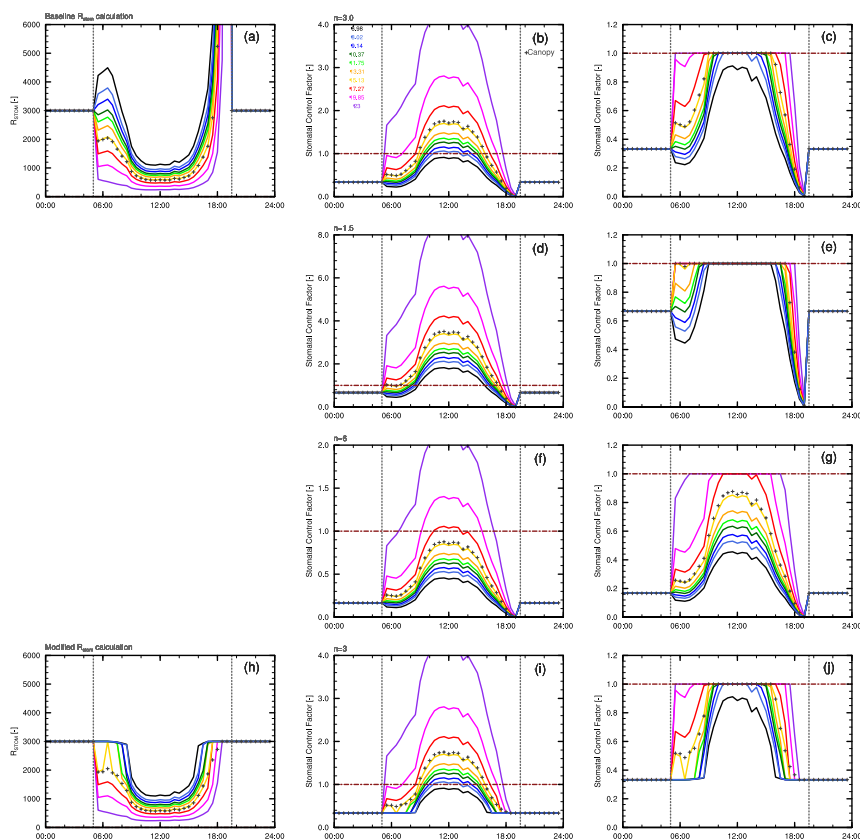
- Acetaldehyde 0.000 0.000
-
- 1 ^aHelmig et al. (1999); ^bGeron et al. (2000)
- 2 Table 6b. Emission factors, ϵ (nmol m^{-2} (projected leaf area) s^{-1}) and total canopy emissions
- 3 ($\text{mg m}^{-2} \text{day}^{-1}$) for methanol and acetaldehyde for the FORCAsT simulations in Table 5.

oVOC	Methanol			Acetaldehyde			
	Simulation	Direct ϵ	Storage ϵ	Total	Direct ϵ	Storage ϵ	Total
E-direct		4.894	0.000	435.8	0.303	0.000	28.7
E-storage		0.000	0.653	457.0	0.000	0.036	28.5
E-combo		1.670	0.418	441.2	0.112	0.027	32.0
E-combo90		2.815	0.296	457.8	0.175	0.019	31.6
S-storage		0.000	0.326	441.0	0.000	0.019	32.1
S-combo		1.065	0.266	454.7	0.063	0.015	31.3
R-storage		0.000	0.653	438.6	0.000	0.040	30.5
R-storageN15		0.000	0.653	429.5	0.000	0.040	31.2
R-storageN6		0.000	0.751	445.6	0.000	0.046	30.9
R-combo		1.670	0.418	434.0	0.112	0.027	31.5
R-comboN15		1.670	0.418	435.8	0.112	0.027	28.7
R-comboN6		1.670	0.418	457.0	0.112	0.027	28.5
S-storageP		0.000	0.326	441.2	0.000	0.019	32.0
S-comboP		1.065	0.266	457.8	0.063	0.015	31.6
R-storageP		0.000	0.653	441.0	0.000	0.040	32.1
R-comboP		1.670	0.418	454.7	0.112	0.027	31.3

4
 5
 6

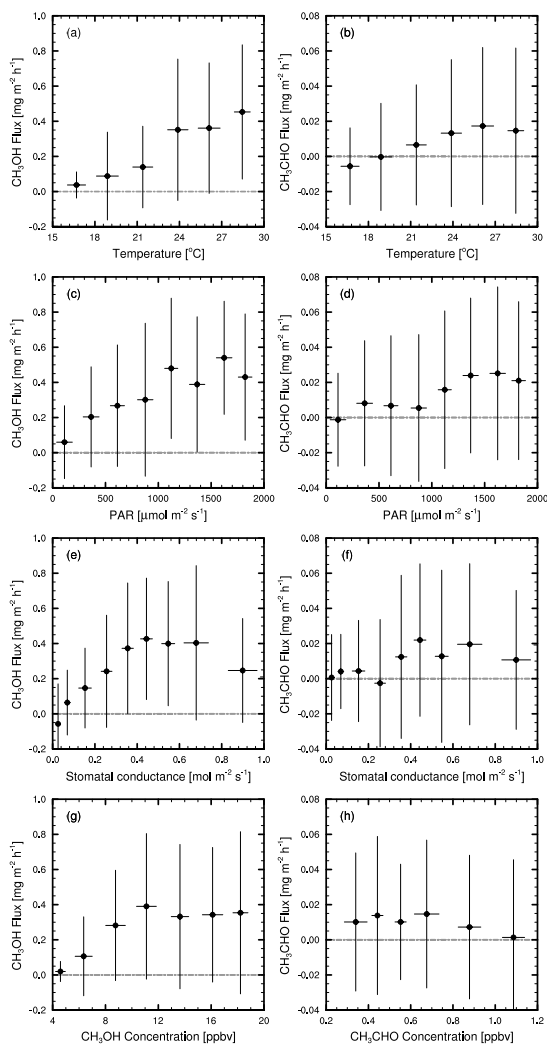


1 Figure 1. Total canopy production and loss rates per unit ground area for methanol (left) and
2 acetaldehyde (right) summed over the 10 crown space layers. Coloured lines show total
3 emissions (top), deposition (middle) and chemical production and loss (bottom) for each
4 simulation.



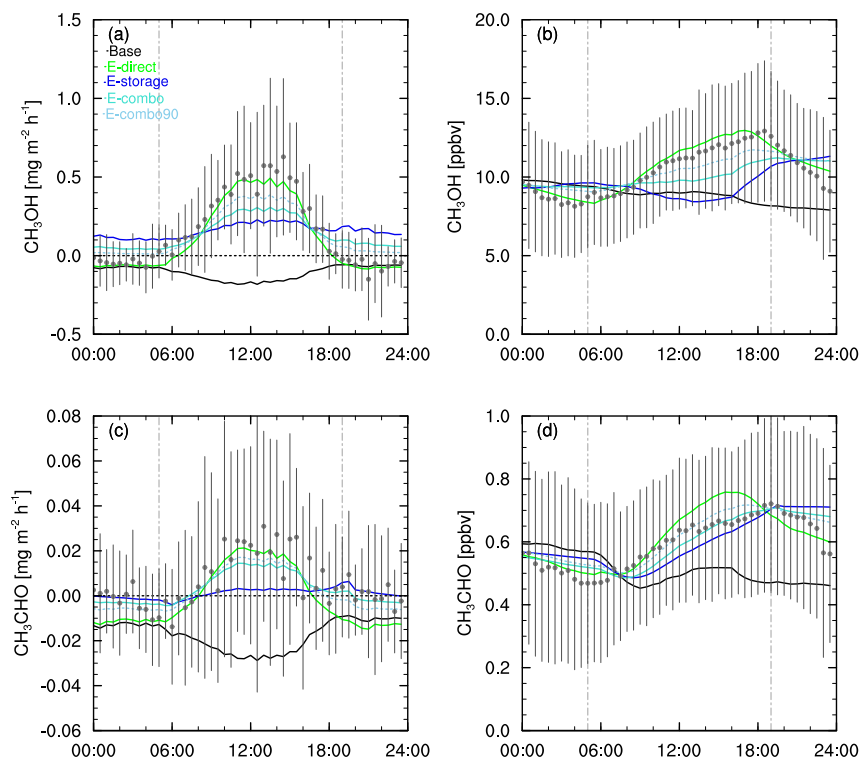
1 Figure 2. Stomatal control applied to storage emissions. The top row shows the baseline (a)
 2 stomatal resistance, (b) stomatal control factor R_{fct} as calculated in Eq. 10, and (c) the
 3 stomatal control factor as calculated in Eqs. 11a and 11b, i.e. with a limiting value of 1.0.
 4 Coloured lines show the resistances and control factors as a leaf area-weighted average for
 5 each crown space model level across the 10 leaf angle classes. The crosses show the canopy
 6 average weighted by foliage fraction in each level. The second and third rows show the effect
 7 on R_{fct} of altering the scaling factor, n , in Eq. 10 ((d) and (f)) and Eqs. 11a and 11b ((e) and
 8 (g)). The bottom row shows the same as the top for the modified stomatal resistance
 9 calculations in which “daylight” is assumed to start only when PAR exceeds a threshold of
 10 $10.0 \mu\text{mol m}^{-2} \text{s}^{-1}$.

11
 12



1 Figure 3. Observed daytime (05:00-19:00 EST) fluxes of methanol (left) for July 2012 versus
2 (a) air temperature, (c) PAR, (e) canopy stomatal conductance, and (g) methanol
3 concentration (all measured at 29 m). The right hand column (panels b, d, f, h) shows the
4 same relationships for acetaldehyde. Temperatures were binned in 2.5 °C intervals, PAR in
5 $250 \mu\text{mol m}^{-2} \text{s}^{-1}$, stomatal conductance in $\sim 0.1 \text{ mol m}^{-2} \text{s}^{-1}$ and concentrations in 2.5 ppbv
6 increments (methanol) and 0.2 ppbv (acetaldehyde). Average values for each bin are marked
7 with circles; vertical and horizontal bars indicate 1 standard deviation above and below the
8 mean in each case.

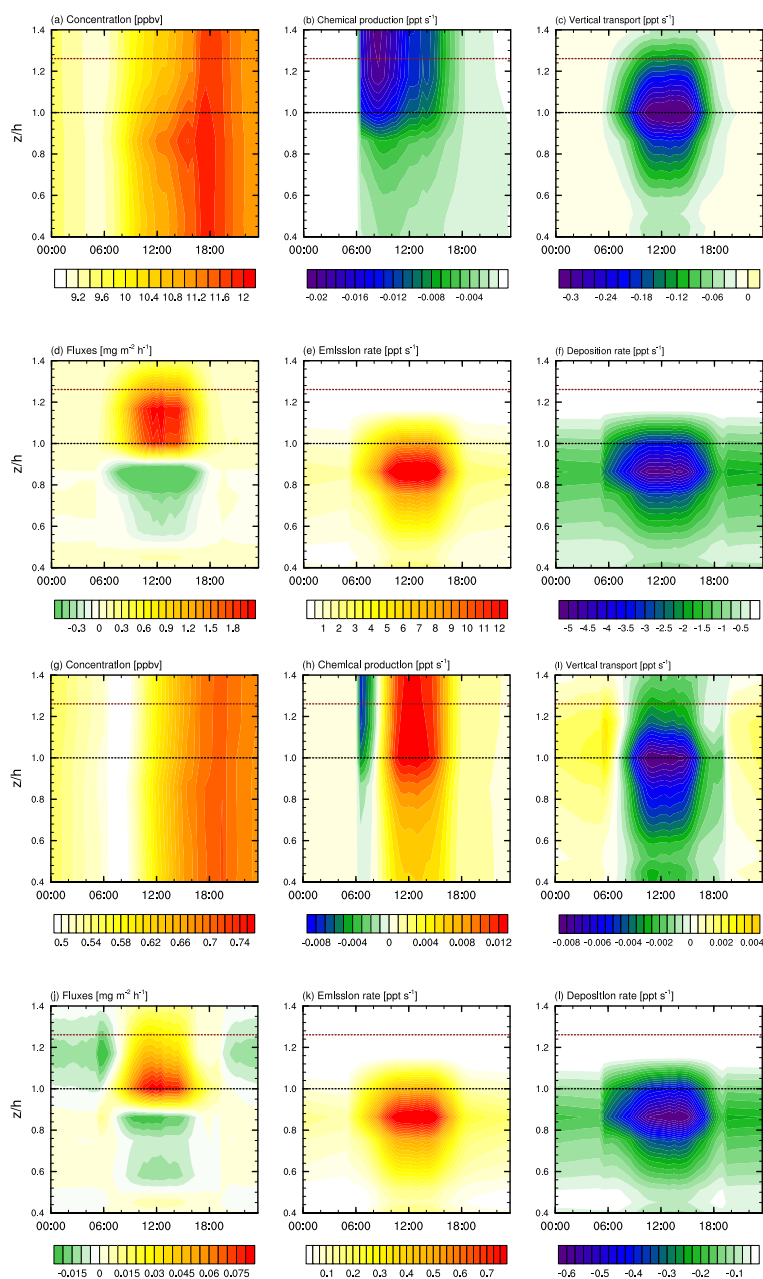
9



1

2 Figure 4. Measured (grey circles with vertical bars indicating 1 standard deviation above and
3 below the mean) and modelled (solid lines) fluxes (left) and concentrations (right) at 29 m for
4 an average day in July 2012 for methanol (a) fluxes ($\text{mg m}^{-2} \text{h}^{-1}$) and (b) concentrations
5 (ppbv), and acetaldehyde (c) fluxes and (d) concentrations. The solid black line shows the
6 baseline model simulation. Coloured lines denote E-direct (green), E-storage (blue) and E-
7 combo (cyan) simulations in which direct, storage and combination emissions pathways
8 respectively are included. The dashed turquoise line shows the E-combo90 (combo emissions
9 with 90% direct and 10% storage emission pathways) sensitivity test. Dashed grey vertical
10 lines show dawn and dusk. Times shown are Eastern Standard Time (EST).

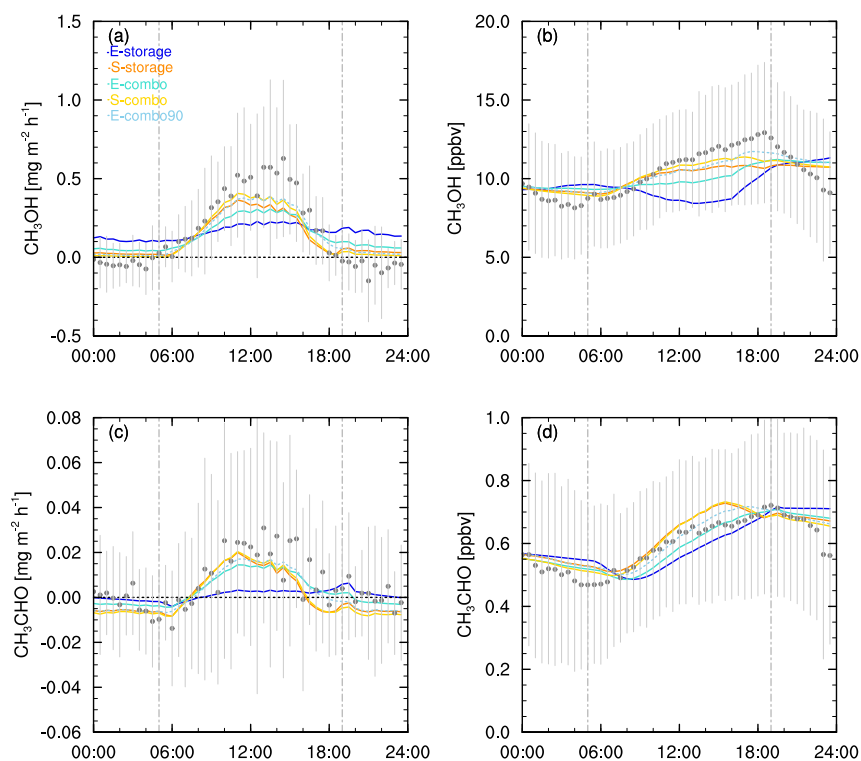
11



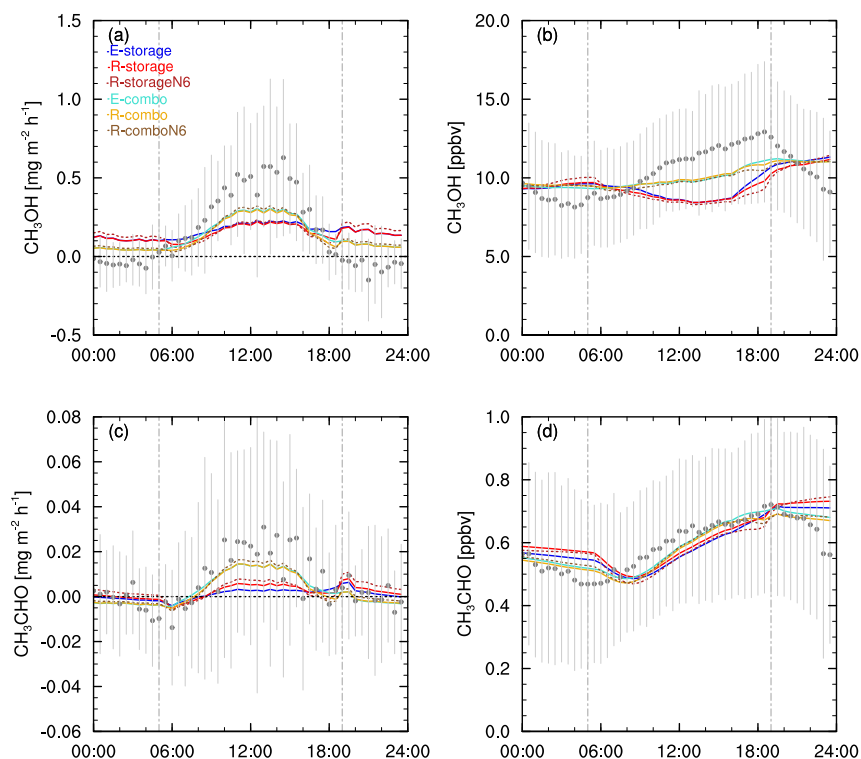
1 Figure 5. Production and loss within the canopy space for methanol: (a) concentration, (b)
2 chemical production rate (including photolysis), (c) changes in concentration due to vertical
3 mixing, (d) fluxes, (e) emission rates, and (f) deposition rates of methanol for the E-combo90



1 simulation. Rates are instantaneous in time and space. The vertical axis shows height relative
2 to canopy top height; times on the horizontal axis are LT. Panels (g)-(l) show the same for
3 acetaldehyde for the E-combo simulation. Dashed horizontal lines denote canopy top (black)
4 and observation height (red).
5



6
7 Figure 6. As Fig. 4 with blue lines showing E-storage and orange lines S-storage simulations,
8 and turquoise and yellow lines showing E-combo and S-combo simulations respectively. The
9 dashed turquoise line shows the E-combo90 sensitivity test. Panels show (a) methanol fluxes,
10 (b) methanol concentrations, (c) acetaldehyde fluxes, and (d) acetaldehyde concentrations at
11 29 m.
12
13
14
15



1

2 Figure 7. Simulations of modified stomatal control of storage emissions (R-). Blue and
3 turquoise lines show E-storage and E-combo as Fig. 6. Red (R-storage) and dashed dark red
4 (R-storageN6) lines show the effects on 100% storage emissions for scaling factor n=3 and
5 n=6 respectively. Gold (R-combo) and dashed brown (R-comboN6) lines show the same for
6 combo emissions (20% storage). Panels show (a) methanol fluxes, (b) methanol
7 concentrations, (c) acetaldehyde fluxes, and (d) acetaldehyde concentrations at 29 m for an
8 average day in July 2012.

9

10

11